Electronic Supplementary Material (ESI) for Chemical Science
This journal is © The Royal Society of Chemistry 2012

Supporting Information for:

A Mononuclear Carboxylate-Rich Oxoiron(IV) Complex - A Structural and Functional Mimic of TauD 'J'

Aidan R. McDonald,[†] Yisong Guo,[§] Van V. Vu,[†] Emile L. Bominaar,[§] Eckard Münck,[§]* Lawrence Que, Jr.[†]**

[†]Department of Chemistry and Center for Metals in Biocatalysis, University of Minnesota, 207 Pleasant Street S.E., Minneapolis, MN 55455

[§]Department of Chemistry, Carnegie Mellon University, Mellon Institute, 4400 Fifth Ave., Pittsburgh, PA 15213

Electronic Supplementary Material (ESI) for Chemical Science
This journal is © The Royal Society of Chemistry 2012

Experimental Section.

Materials. All reactions with air-sensitive materials were conducted under an inert atmosphere using either standard Schlenk techniques or a nitrogen atmosphere glove box. All reagents and solvents were purchased from commercial sources and used as received, unless otherwise stated. Dichloromethane (CH_2Cl_2) was purified using a VAC solvent purification set-up. Methanol (CH_3OH) was purified by refluxing over metallic magnesium and subsequent distillation. Bis-(2-pyridyl)-methylamine (**1(a)**, DPMA)[1] and 2-(*tert*-butylsulfonyl)-iodosylbenzene (soluble iodosylbenzene, ^{s}ArIO)[2] were prepared according to literature procedures. 3-chloroperoxybenzoic acid was purified according to literature procedures.[3] $[Fe^{II}(N4Py)](ClO_4)_2$ was synthesized according to literature procedures.[4, 5]

1',1'-bis(2-pyridyl)pentylamine, **^{n}Bu-DPMA 1(b)**. To a stirring solution of bis-(2-pyridyl)-methylamine (1.14 g, 6.16 mmol) in tetrahydrofuran (20 mL) cooled to -78 °C (acetone, dry ice) was added 1-butyllithium (2.46 mL of a 2.5 M solution in hexanes, 6.16 mmol). The resulting solution was stirred at -78 °C for 2 h, and then allowed to warm to room temperature slowly. 1-Bromobutane (0.84 g, 6.16 mmol) was added and the resulting solution was stirred at room temperature for 72 h. Water (10 mL) was added to quench the reaction. The resulting aqueous solution was extracted with CH_2Cl_2 (30 mL, 3x) and the organic layer was dried over $MgSO_4$. Removal of the CH_2Cl_2 and volatile byproducts in vacuo yielded the desired product in quantitative yield as a colorless oil. ^{1}H NMR ($CDCl_3$, 500 MHz): δ = 0.84 (t, 3H), 1.17 (m, 2H), 1.31 (m, 2H), 2.37 (m, 2H), 2.53 (s, 2H), 7.07 (m, 2H), 7.50 (d, 2H) 7.58 (t, 2H) 8.52 (d, 2H); ^{13}C NMR ($CDCl_3$, 125 MHz) δ = 14.1, 23.2, 26.1, 41.0, 64.0, 121.1, 121.3, 136.3, 148.5, 165.7. ESI-MS: calcd. for $C_{15}H_{20}N_3$ ($[^{n}$Bu-DPMA$](H)^{+}$), m/z = 242.2. Anal. Calcd. for $C_{15}H_{19}N_3$: C, 74.65; H, 7.94; N, 17.41 Found: C, 74.14; H, 7.65; N, 17.08.

General procedure for the preparation of compounds Et_2P2DA and $Et_2{}^{n}$Bu-P2DA. In a typical experiment the requisite bis-(2-pyridyl)methylamine compound (6 mmol) was

This journal is © The Royal Society of Chemistry 2012

dissolved in acetonitrile (CH_3CN, 30 mL). To this was added potassium carbonate (3.32 g, 24 mmol) and ethyliodoacetate (3.85 g, 18 mmol). The resulting mixture was stirred at reflux under an inert atmosphere for 5 days. After cooling to room temperature the solution was filtered over a glass frit to remove inorganic salts and the CH_3CN was subsequently removed in vacuo. The resulting residue was dissolved in ethylacetate (30 mL) and washed with water (3 x 20 mL) and subsequently dried over magnesium sulfate followed by solvent removal in vacuo to yield a viscous brown residue. Column chromatography yielded the desired product.

Diethyl-N-(1',1'-bis-(2-pyridyl)methyl)iminodiacetate, *Et_2P2DA*. Chromatography on a silica gel column (Ethylacetate/Triethylamine, 9:1) yielded the desired product as a pale orange oil (55% yield). ^{1}H NMR ($CDCl_3$, 300 MHz): δ = 1.22 (t, 6H), 3.62 (s, 4H), 4.13 (d, 4H), 5.60 (s, 1H), 7.14 (d, 2H), 7.70 (m, 4H), 8.53 (d, 2H); ^{13}C NMR ($CDCl_3$, 75MHz) δ = 14.27, 52.71, 60.52, 73.58, 122.53, 123.95, 138.88, 149.39, 160.12, 171.44. IR (cm^{-1}) 1741, 1588, 1434. ESI-MS: calcd. for $C_{19}H_{24}N_3O_4Na$ ($[Et_2P2DA](Na)^+$), m/z = 380.11. Anal. Calcd. for: $C_{19}H_{23}N_3O_4$ C, 63.85; H, 6.49; N, 11.76; Found: C, 63.40; H, 6.95; N, 10.41.

Diethyl-N-(1',1'-bis-(2-pyridyl)pentyl)iminodiacetate, *$Et_2{}^n$Bu-P2DA*. Chromatography on a basic alumina column (Beckmann Grade 1, hexanes/diethylether, 3:2) yielded the desired product as a colorless oil (yield = 18%). ^{1}H NMR ($CDCl_3$, 300 MHz): δ = 0.71 (t, 3H), 0.89 (m, 2H), 1.18 (m, 8H), 2.44 (m, 2H), 3.56 (s, 4H), 4.02 (dd, 4H), 7.11 (m, 2H), 7.60-7.72 (m, 4H), 8.52 (d, 2H); ^{13}C NMR ($CDCl_3$, 75MHz) δ = 14.1, 14.2, 23.2, 26.3, 37.9, 52.3, 60.4, 74.1, 121.6, 123.6, 135.6, 148.1, 161.7, 172.0. IR (cm^{-1}) 1748, 1587, 1429. ESI-MS: calcd. for $C_{23}H_{32}N_3O_4$ ($[Et_2{}^n$Bu-P2DA$](H)^+$), m/z = 414.3. Anal. Calcd. for $C_{23}H_{31}N_3O_4$: C, 66.81; H, 7.56; N, 10.16; Found: C, 66.53; H, 7.46; N, 10.06.

General procedure for the preparation of compounds ***2(a)*** *K_2P2DA and* ***2(b)*** *$K_2{}^n$Bu-P2DA.*

In a typical experiment the requisite diethyl-*N*-(1',1'-bis-(2-pyridyl)methyl)iminodiacetate compound (1 mmol) was dissolved in

This journal is © The Royal Society of Chemistry 2012

tetrahydrofuran/water (30 mL, 1:1). To this was added potassium hydroxide (0.112 g, 2 mmol). The resulting solution was stirred at room temperature for 16 h. Solvent was subsequently removed in vacuo yielding an oily residue. Acetone (10 mL) was added resulting in the formation of a white precipitate. The acetone was subsequently removed under vacuum. This step was repeated 3 times to yield the desired dipotassium salts as a white powder. These compounds are very hygroscopic and must be stored under an inert atmosphere.

Dipotassium-N-(1',1'-bis-(2-pyridyl)methyl)iminodiacetate, **K_2P2DA 2(a)**. ^{1}H NMR (D_2O, 300 MHz): δ = 3.08 (s, 4H), 5.45 (s, 1H), 7.08 (t, 2H), 7.62 (m, 4H), 8.18 (d, 2H); ^{13}C NMR (D_2O, 75MHz) δ = 54.7, 71.8, 122.9, 123.9, 138.1, 148.3, 159.1, 179.5. IR (cm^{-1}) 1598, 1589, 1398. ESI-MS: calcd. for $C_{15}H_{16}N_3O_4$ ($[P2DAH_2](H)^+$, compound was acidified with aq. HCl for ESI-MS experiment) m/z = 302.1. Anal. Calcd. for $C_{15}H_{17}N_3O_6K_2$: C, 43.57; H, 4.14; N, 10.16; Found: C, 43.57; H, 4.17; N, 9.83.

Dipotassium-N-(1',1'-bis-(2-pyridyl)pentyl)iminodiacetate, **$K_2{}^n$Bu-P2DA 2(b)**. ^{1}H NMR (CD_3OD, 300 MHz): δ = 0.72 (m, 5H), 1.18 (m, 2H), 2.39 (m, 2H), 2.92 (s, 4H), 7.22 (d, 2H), 7.29 (m, 2H), 7.75 (t, 2H) 8.70 (d, 2H); ^{13}C NMR (CD_3OD, 75MHz) δ = 13.0, 22.8, 27.8, 37.7, 57.5, 75.6, 121.7, 125.2, 135.1, 148.4, 159.3, 179.0. IR (cm^{-1}) 1602, 1579, 1400. ESI-MS: calcd. for $C_{19}H_{24}N_3O_4$ ($[H_2{}^n$Bu-P2DA$](H)^+$, compound was acidified with aq. HCl for ESI-MS experiment), m/z = 358.2. Anal. Calcd. for $C_{19}H_{30}N_3O_7K_3$: C, 43.41; H, 4.98; N, 7.99; Found: C, 43.33; H, 4.89; N, 7.85.

Potassium-N-(1',1'-bis-(2-pyridyl)methyl)iminodiacetato-hydroxo-iron(II), **[Fe^{II}(P2DA)] 3(a)**. Dipotassium-*N*-(1',1'-bis-(2-pyridyl)methyl)iminodiacetate (0.1 g, 0.27 mmol) was dissolved in CH_3OH (5 mL). To this was added a solution of $FeCl_2$ (0.034 g, 0.27 mmol) in CH_3OH (2 mL). An immediate color change from colorless to dark red was observed followed by the precipitation of a red crystalline material. The red material was isolated by vacuum filtration (yielding an almost colorless filtrate) followed by washing with CH_3OH (5 mL, 2x) and diethylether (5 mL, 2x) (Yield: 80%). The red material was soluble in water but insoluble in CH_3OH and CH_2Cl_2. ^{1}H NMR (D_2O, 300 MHz): -2.3,

This journal is © The Royal Society of Chemistry 2012

0.8, 28.2, 41.7, 54.7, 61.6, 137.8. ESI-MS: calcd. for $C_{15}H_{13}FeKN_3O_4$ ($[Fe^{II}(P2DA)](K)^+$), m/z = 394.2. IR (cm^{-1}) 1630-1590 broad, 1375 broad. Anal. Calcd. for $C_{15}H_{14}N_3O_5FeK$: C, 43.81; H, 3.43; N, 10.22; Found: C, 43.76; H, 3.99; N, 9.92.

Tetra-1-butylammonium-N-(1',1'-bis-(2-pyridyl)pentyl)iminodiacetato-chloro-iron(II), **$[Fe^{II}(Cl)(^nBu\text{-}P2DA)]N^nBu_4$, 3(b)-Cl**.

Dipotassium-*N*-(1',1'-bis-(2-pyridyl)pentyl)iminodiacetate (0.13 g, 0.31 mmol) was dissolved in CH_3OH (3 mL). To this was added a solution of $FeCl_2$ (0.037 g, 0.29 mmol) in CH_3OH (2 mL) which resulted in an immediate color change from colorless to dark purple. After 1 min. of stirring at room temperature, the solution was poured onto diethylether (100 mL) resulting in the formation of a purple precipitate which was collected by vacuum filtration. The purple precipitate (**$[Fe^{II}(Cl)(^nBu\text{-}P2DA)]K$**) was dissolved in CH_2Cl_2 (10 mL) and filtered over celite to remove remnant insoluble materials. To the CH_2Cl_2 solution was added ($^nBu_4N$)Cl (0.08 g, 0.29 mmol) and the resulting solution was stirred at room temperature for 2 h. The solution was then filtered over celite to remove insoluble materials and then poured onto diethylether (100 mL) to yield a dark purple crystalline which was collected by vacuum filtration (yield = 73% of **$[Fe^{II}(Cl)(^nBu\text{-}P2DA)]N^nBu_4$**). Alternatively ($Ph_4P$)Cl (0.11 g, 0.29 mmol) was added in place of ($^nBu_4N$)Cl to give **$[Fe^{II}(Cl)(^nBu\text{-}P2DA)]PPh_4$** using the same work-up procedures. ^1H NMR (of K^+ salt) (CD_2Cl_2, 300 MHz): -4.7, 0.8, 0.5, 7.0, 25.5, 26.0, 49.8, 52.8, 57.7, 152.2. ESI-MS: calcd. for $C_{19}H_{21}N_3O_4FeCl$ ($[Fe^{II}(Cl)(^nBu\text{-}P2DA)]^-$, m/z = 446.5. IR ($cm^{-1}$) 1631, 1598, 1380. Anal. Calcd. for N^nBu_4 salt: $C_{37}H_{61}Cl_5FeN_4O_4$ C, 51.73; H, 7.16; N, 6.52 Found: C, 51.57; H, 7.09; N, 6.69.

*Ligand substitution Reactions with **3(b)-Cl**:*

Hydroxide: To a CH_2Cl_2 solution of **3(b)-Cl** (1 mmol/L) cooled to -95 °C was added 10 equivalents of ($^nBu_4N$)OH in CH_3OH. The reaction was monitored using electronic absorption spectroscopy and ESI-MS. The formed complex was stable at room temperature.

N-Heterocyclic Amines: To a CH_2Cl_2 solution of **3(b)-Cl** (1 mmol/L) cooled to -95 °C was added 100 equivalents of N-heterocyclic amine in CH_2Cl_2. The reaction was

This journal is © The Royal Society of Chemistry 2012

monitored using electronic absorption spectroscopy. N-heterocyclic amines that demonstrated a change in the UV-vis absorption spectrum upon addition to **3(b)-Cl** were: pyridine, 4-chloropyridine, 4-methoxypyridine, 4-picoline, 4-dimethylaminopyridine, 1-methylimidazole, 1,2-dimethylimidazole, 1,2,4,5-tetramethylimidazole, 1-methylbenzimidazole, 1-methylpyrazole. However, 2,6-lutidine and collidine did not effect a change in the UV-vis properties, and are thus assumed not to displace the chloride ligand. The formed N-heterocyclic amine adducts were less stable than **3(b)-Cl** at room temperature. Upon warming to room temparature a red precipitate that was insoluble in common organic solvents formed. **3(b)-Me$_2$Im** (Me_2Im = 1,2-dimethylimidazole) was sufficiently stable at room temperature to allow NMR analysis: ^{1}H NMR (**3(b)-Me$_2$Im**) (CD_2Cl_2, 300 MHz): -6.5, -1.1, 19.3, 23.9, 30.0, 40.9, 43.3, 46.4, 48.0, 50.9, 51.1, 53.9, 131.2, 151.2.

*Generation of [(Fe^{III})$_2$(O)(P2DA)$_2$] (**4(a)**) and [(Fe^{III})$_2$(O)(^{n}Bu-P2DA)$_2$], (**4(b)**):*

4(a): An aqueous solution of **3(a)** was exposed to air resulting in a color change from pale yellow to pale orange. The resulting pale orange solution was allowed to sit at room temperature for 1 week resulting in the formation of orange crystals of **4(a)**. IR (cm^{-1}) 1640, 1608, 1355. ESI-MS calcd. for $C_{30}H_{26}Fe_2KN_6O_9$, m/z = 765.1.

4(b): A dichloromethane solution of **3(b)-Cl** was exposed to air resulting in a color change from dark red to pale orange. Diethylether was added to the resulting pale orange solution and the resulting solution was allowed to sit for 1 week at room temperature resulting in the formation of orange crystals of **4(b)**. IR (cm^{-1}) 1645, 1597, 1342. ESI-MS calcd. for $C_{38}H_{42}Fe_2KN_6O_9$, m/z = 877.0.

*Generation of [Fe^{IV}(O)(^{n}Bu-P2DA)], **5(b)**:*

Method A. At room temperature, 1,2-dimethylimidazole (500 equivalents) was added to a CH_2Cl_2 solution of **3(b)-Cl** (1 mmol/L). The resulting solution was cooled rapidly to -95 °C and 2-(*tert*-butylsulfonyl)-iodosylbenzene (3 equiv.) in CH_2Cl_2 was added to yield [Fe^{IV}(O)(^{n}Bu-P2DA)] in 80% yield. *Method B*. At room temperature, 1,2-dimethylimidazole (500 equivalents) was added to a CH_3OH solution of **3(b)-Cl** (1 mmol/L). The resulting solution was cooled rapidly to -95 °C and 3-chloroperoxybenzoic

This journal is © The Royal Society of Chemistry 2012

acid (3 equiv.) in CH_3OH was subsequently added to yield $[Fe^{IV}(O)(^{n}Bu\text{-}P2DA)]$ in 90% yield.

Reactivity Studies:

We investigated the reactivity of **5(b)** by preparing it at -95 °C and then transferring the solution to a separate spectrometer cooled to -60 °C due to the low reactivity of **5(b)** towards common substrates at -95 °C. A methanol solution of **5(b)** (1 mmol) prepared using the aforementioned method B was transferred via cooled syringe to a reaction vessel cooled to -60 °C and allowed to equilibrate at -60 °C for 3 minutes. For consistency, a methanol solution of $[Fe^{IV}(O)(N4Py)]^{2+}$ (1 mmol) in the presence of 500 equivalents of Me_2Im was generated by exposure of $[Fe^{II}(N4Py)]^{2+}$ in methanol (1 mmol) at -60 °C to 3 equivalents *m*-CPBA. Kinetic studies were performed by adding appropriate amounts of substrates to **5(b)** or $[Fe^{IV}(O)(N4Py)]^{2+}$ at -60 °C and monitoring the reaction using a UV-vis spectrophotometer. Rate constants, k_{obs}, were obtained by pseudo-first-order fitting of the decrease of the Fe^{IV}=O chromophore at λ_{max} = 770 nm (**5(b)**) or λ_{max} = 695 nm ($[Fe^{IV}(O)(N4Py)]^{2+}$) . Second order rate constants were obtained from concentration dependent data. The reactivity of 1-methyl-2,5-cyclohexadiene, and ferrocene towards **5(b)** and $[Fe^{IV}(O)(N4Py)]^{2+}$ was investigated. The formation of ferrocenium from ferrocene was confirmed by UV-vis and EPR spectroscopies, while ^{1}H NMR and GC-MS analyses were utilized to confirm the formation of toluene from 1-methyl-2,5-cyclohexadiene and ^{31}P NMR was utilized to confirm the formation of methyldiphenylphosphine oxide from methyldiphenylphosphine.

*X-ray crystal structure determination of compounds **3(b)-Cl**, **4(a)**, **4(b)**.*

$[Fe^{II}(Cl)(^{n}Bu\text{-}P2DA)]PPh_4$: A crystal (approximate dimensions 0.45x 0.40 x 0.03mm^3) was placed onto the tip of a 0.1 mm diameter glass capillary and mounted on a CCD area detector diffractometer for a data collection at 123(2) K.[6] A preliminary set of cell constants was calculated from reflections harvested from three sets of 20 frames. These initial sets of frames were oriented such that orthogonal wedges of reciprocal space were surveyed. This produced initial orientation matrices determined from 154 reflections. The data collection was carried out using MoKα radiation (graphite monochromator) with a frame time of 90 seconds and a detector distance of 4.8 cm. A randomly oriented region

This journal is © The Royal Society of Chemistry 2012

of reciprocal space was surveyed to the extent of one sphere and to a resolution of 0.84 Å. Four major sections of frames were collected with 0.30º steps in ω at four different φ settings and a detector position of -28º in 2θ. The intensity data were corrected for absorption and decay (SADABS).[7] Final cell constants were calculated from 2936 strong reflections from the actual data collection after integration (SAINT).[8] Please refer to Table 1 for additional crystal and refinement information. The structure was solved using Bruker SHELXTL[9] and refined using Bruker SHELXTL.[9] The space group P21/c was determined based on systematic absences and intensity statistics. A direct-methods solution was calculated which provided most non-hydrogen atoms from the E-map. Full-matrix least squares/difference Fourier cycles were performed which located the remaining non-hydrogen atoms. All non-hydrogen atoms were refined with anisotropic displacement parameters. All hydrogen atoms were placed in ideal positions and refined as riding atoms with relative isotropic displacement parameters. The final full matrix least squares refinement converged to $R1 = 0.0667$ and $wR2 = 0.1973$ (F^2, obs. data).

4(a) $[Fe^{III}_2(O)(P2DA)_2]$. A crystal (approximate dimensions 0.25 x 0.08 x 0.05 mm^3) was placed onto the tip of a 0.1 mm diameter glass capillary and mounted on a Bruker SMART Platform CCD diffractometer for a data collection at 173(2) K.[6] A preliminary set of cell constants was calculated from reflections harvested from three sets of 20 frames. These initial sets of frames were oriented such that orthogonal wedges of reciprocal space were surveyed. This produced initial orientation matrices determined from 13 reflections. The data collection was carried out using MoKα radiation (graphite monochromator) with a frame time of 90 seconds and a detector distance of 4.9 cm. A randomly oriented region of reciprocal space was surveyed to the extent of one sphere and to a resolution of 0.84 Å. Three major sections of frames were collected with 0.50º steps in ω at three different φ settings and a detector position of -28º in 2θ. The intensity data were corrected for absorption and decay (SADABS).[7] Final cell constants were calculated from the xyz centroids of 2637 strong reflections from the actual data collection after integration (SAINT).[8] Please refer to Table 1 for additional crystal and refinement information. The structure was solved using SHELXS-97[9] and refined using SHELXL-97.[9] The space group C2/c was determined based on systematic absences and

This journal is © The Royal Society of Chemistry 2012

intensity statistics. A direct-methods solution was calculated which provided most non-hydrogen atoms from the E-map. Full-matrix least squares/difference Fourier cycles were performed which located the remaining non-hydrogen atoms. All non-hydrogen atoms were refined with anisotropic displacement parameters. All hydrogen atoms were placed in ideal positions and refined as riding atoms with relative isotropic displacement parameters. The function SQUEEZE, in the program PLATON[10], was used to model the electron density of disordered solvent molecules in a solvent channel. A void space of 1069.5 $Å^3$ (28.8% of the cell volume), containing 241 electrons per cell, was found. The final full matrix least squares refinement converged to $R1 = 0.0347$ and $wR2 = 0.0835$ (F^2, all data).

4(b), $[Fe^{III}_2(O)(^nBu\text{-}P2DA)_2]$. A clear light red block-like specimen of $C_{41}H_{55}Fe_2N_6O_{12}$, approximate dimensions 0.100 mm x 0.150 mm x 0.250 mm, was used for the X-ray crystallographic analysis. The X-ray intensity data were measured. A total of 2080 frames were collected. The total exposure time was 17.33 hours. The frames were integrated with the Bruker SAINT software package using a narrow-frame algorithm.[8] The integration of the data using a monoclinic unit cell yielded a total of 19624 reflections to a maximum θ angle of 25.68° (0.82 Å resolution), of which 4400 were independent (average redundancy 4.460, completeness = 99.8%, R_{int} = 8.35%, R_{sig} = 7.41%) and 3164 (71.91%) were greater than $2\sigma(F^2)$. The final cell constants of $\underline{a}$ = 24.8834(18) Å, $\underline{b}$ = 8.8381(5) Å, $\underline{c}$ = 24.4677(12) Å, β = 120.136(3)°, volume = 4653.7(5) $Å^3$, are based upon the refinement of the XYZ-centroids of 2582 reflections above 20 σ(I) with 4.982° < 2θ < 40.82°. Data were corrected for absorption effects using the multi-scan method (SADABS).[7] The ratio of minimum to maximum apparent transmission was 0.803. The calculated minimum and maximum transmission coefficients (based on crystal size) are 0.8470 and 0.9345.

The structure was solved and refined using the Bruker SHELXTL Software Package,[9] using the space group C 1 2/c 1, with Z = 4 for the formula unit, $C_{41}H_{55}Fe_2N_6O_{12}$. The final anisotropic full-matrix least-squares refinement on F^2 with 308 variables converged at R1 = 5.55%, for the observed data and wR2 = 15.98% for all data. The goodness-of-fit

This journal is © The Royal Society of Chemistry 2012

was 1.043. The largest peak in the final difference electron density synthesis was 0.991 $e^-/Å^3$ and the largest hole was -0.416 $e^-/Å^3$ with an RMS deviation of 0.086 $e^-/Å^3$. On the basis of the final model, the calculated density was 1.335 g/cm^3 and F(000), 1964 e^-.

Table S1. Crystal data and structure refinement for complexes **3(b)**, **4(a)**, **4(b)**.

	3(b)-Cl, $[Fe^{II}(Cl)(^nBu\text{-}P2DA)]PPh_4$		**4(a), $[Fe^{III}_2(O)(P2DA)_2]$**		**4(b), $[Fe^{III}_2(O)(^nBu\text{-}P2DA)_2]$**	
Empirical formula	$C_{45}H_{45}Cl_5FeN_3O_4P$		$C_{30}H_{26}Fe_2N_6O_9$		$C_{41}H_{55}Fe_2N_6O_{12}$	
Formula weight	955.91		726.27		953.61	
Temperature	123(2)		173(2) K		173(2) K	
Crystal system	Monoclinic		Monoclinic		monoclinic	
Space group	$P2_1/c$		C2/c		C 1 2/1 1	
Unit cell dimensions	*a* = 19.234(5) Å	α = 90°	*a* = 18.810(3) Å	α = 90°	a = 24.8834(18) Å 136(3)°	α = 90°
	b = 14.717(3) Å	β = 107.866(3)°	*b* = 8.8413(12) Å	β = 109.478 (2)°	b = 8.8381(5) Å	β = 120.
	c = 16.801(4)Å	γ = 90°	*c* = 23.661(3) Å	γ = 90°	c = 24.4677(12) Å	γ = 90°
Volume	4526.4(18) $Å^3$		3709.8(9) $Å^3$		4653.7(5) $Å^3$	
Z	4		4		4	
Density (calculated)	1.403 mg/m^3		1.300 mg/m^3		1.335 Mg/cm^3	
Crystal color,	Red, plate		Orange Needle		clear light red block	

This journal is © The Royal Society of Chemistry 2012

morphology			
Crystal size	0.45 x 0.40 x 0.03 mm^3	0.25 x 0.08 x 0.05 mm^3	0.100 x 0.150 x 0.250 mm
Goodness-of-fit on F^2	1.105	1.006	1.043
Final *R* indices [$I > 2\text{sigma}(I)$]	*R*1 = 0.0667, *wR*2 = 0.1669	*R*1 = 0.0484, *wR*2 = 0.0799	R1 = 0.0555, wR2 = 0.1404
R indices (all data)	*R*1 = 0.1109, *wR*2 = 0.1973	*R*1 = 0.0484, *wR*2 = 0.0835	R1 = 0.0822, wR2 = 0.1598

Physical Methods. Electronic absorption spectra were recorded on a Hewlett-Packard (Agilent) 8453 diode array spectrophotometer (190-1100 nm range) in quartz cuvettes cooled using a liquid nitrogen cooled cryostat from Unisoku Scientific Instruments (Osaka, Japan). Mössbauer spectra were recorded using a Janis Research Super-Varitemp dewar that allowed studies in applied magnetic fields up to 8.0 T in a temperature range of 1.5 to 200 K. Mössbauer spectral simulations were performed using the WMOSS software package (SEE Co., Edina, MN). Isomer shifts are quoted relative to Fe metal at 298 K. High-resolution electrospray mass spectrometry was performed using a Bruker Bio-TOF II spectrometer. Metastable species were infused directly into the instrument using a pre-chilled gas-tight syringe. Fourier transform infra-red transmission spectra were recorded at room temperature on solid samples, on a Thermo-Nicolet Avatar 370 FT-IR.

XAS Studies: X-ray Absorption Spectroscopy (XAS) data were collected on beamline X3B at the National Synchrotron Lightsource of Brookhaven National Laboratory (NSLS). The synchrotron ring was operated at 2.8 GeV and 100-300 mA beam current and a Si(111) double crystal monochromator was used. Fluorescence data were collected over the energy range of 6.8 - 8.0 keV using a 13-element Ge detector. The beam spot size on samples was 5.0 mm (horizontal) x 1.0 mm (vertical) for **3(b)-Cl** and **3(b)-Me_2Im**. Three identical samples of **5(b)** were prepared in tandem Mössbauer/XAS cups

This journal is © The Royal Society of Chemistry 2012

with large windows that allowed 8 spots of 4.5 mm x 1.0 mm. Spectra of an iron foil were collected concomitantly with the samples and were used as internal reference, the first inflection points of which were set to 7112.00 eV.

Standard procedures were used to reduce, average and process the raw data using the EXAFSPAK package.[11] Data normalization was carried out using Athena program[12] or MBACK program.[13] Pre-edge quantification was carried out with Edg_Fit program of EXAFSPAK using a standard procedure.[14] Opt program of EXAFSPAK was used to fit EXAFS data. Theoretical EXAFS amplitude and phase functions were calculated using the FEFF package (version 8.4).[15] The input models for FEFF calculation were built based on the crystal structure of **3(b)-Cl**. The parameters r and σ^2 were floated, while N was kept fixed for each fit and systematically varied in integer steps between fits. Scale factor was fixed at 0.9 and threshold energy (E_0) was varied but maintained at a common value for all shells

DFT calculations: DFT calculations were performed using Becke's three parameter hybrid (B3LYP) functional and basis set 6-311G provided by Gaussian'09 software package.[16] The initial structural model for **5(b)** was constructed using the crystal structure of **3(b)-Cl** by replacing the $^{-}$Cl ligand with an oxygen atom at the axial position, and the initial structural model for $[Fe^{IV}(O)(N4Py)]^{2+}$ was taken from the published crystal structure.[17] The SCF procedure and geometry optimization were terminated upon reaching the default convergence criteria. The corrections of zero-point, thermal, enthalpic and entropic energies, as well as the solvation energy calculated using the polarizable continuum model (PCM) were all calculated based on the optimized structures of both spin states ($S = 1$ and $S = 2$) of **5(b)** and $[Fe^{IV}(O)(N4Py)]^{2+}$ obtained by the gas-phase calculations. The solvent used in the calculations was methanol. The quadrupole splitting ΔE_Q was calculated using the property keyword of the Gaussian code and $Q(^{57}Fe) = 0.17$ barn. The ^{57}Fe isomer shift δ was evaluated from the DFT charge density at the Fe nucleus using the calibration given by Vrajmasu et al..[18] The populations were calculated with the population keyword.

This journal is © The Royal Society of Chemistry 2012

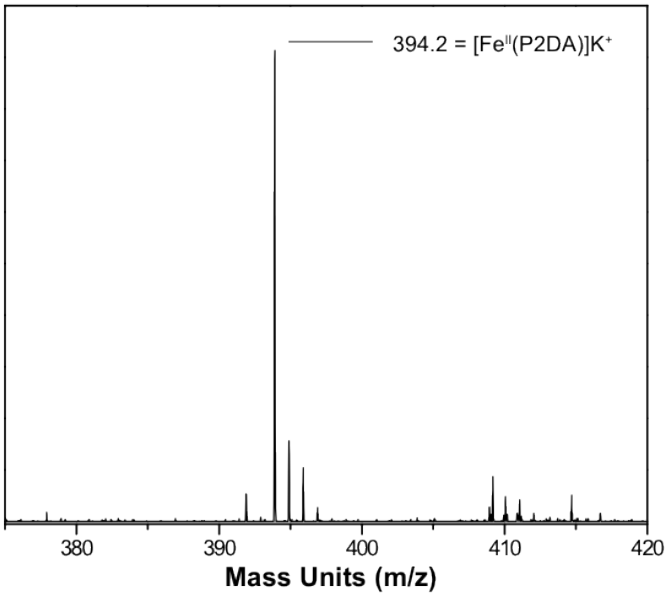

Figure S1. ESI-MS Spectrum of compound **3(a)**. m/z = 394.2 corresponding to $[Fe^{II}(P2DA)](K)^{+}$.

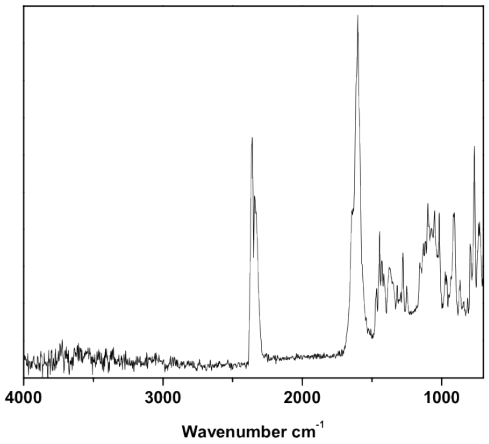

Figure S2. FT-IR spectrum of **3(a)**. Broad signals at ~1620 and ~1370 cm^{-1} assigned to the symmetric and asymmetric vibrations of the carboxylate moieties.

This journal is © The Royal Society of Chemistry 2012

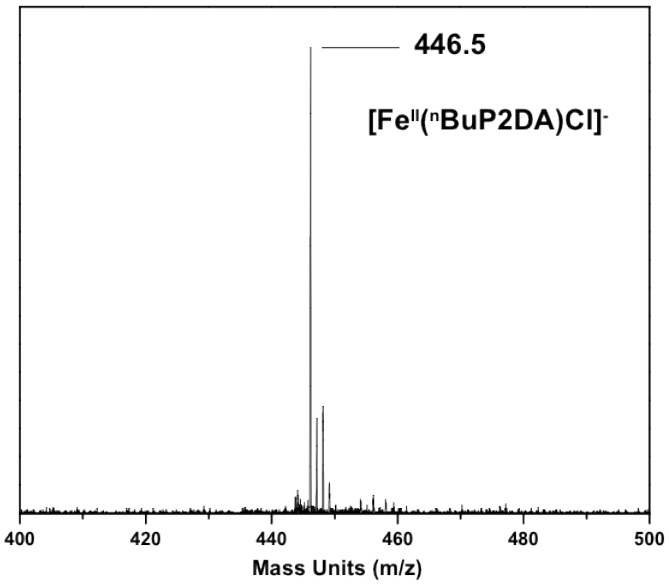

Figure S3. ESI-MS spectrum of **3(b)-Cl**.

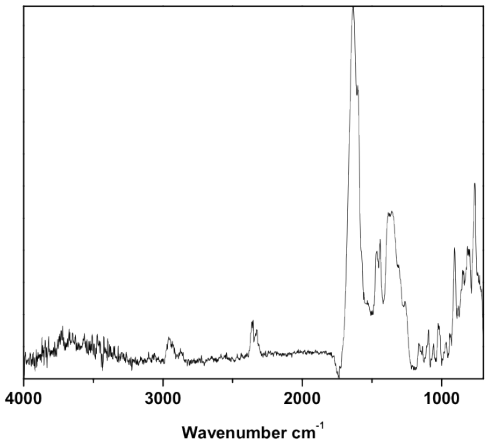

Figure S4. FT-IR spectrum of **3(b)-Cl**. Resonances at ν = 1631 and 1380 cm^{-1} assigned to the asymmetric and symmetric carboxylate vibrations.

This journal is © The Royal Society of Chemistry 2012

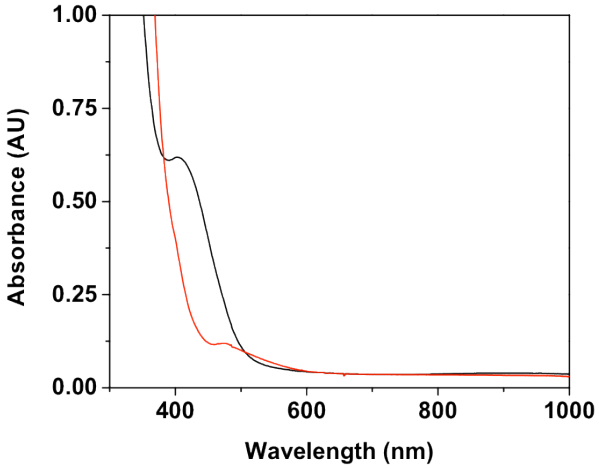

Figure S5. UV-vis absorption spectra of compound **3(a)** (1 mmol/L, H_2O, black trace) and compound **4(a)** (1 mmol/L, H_2O, red trace).

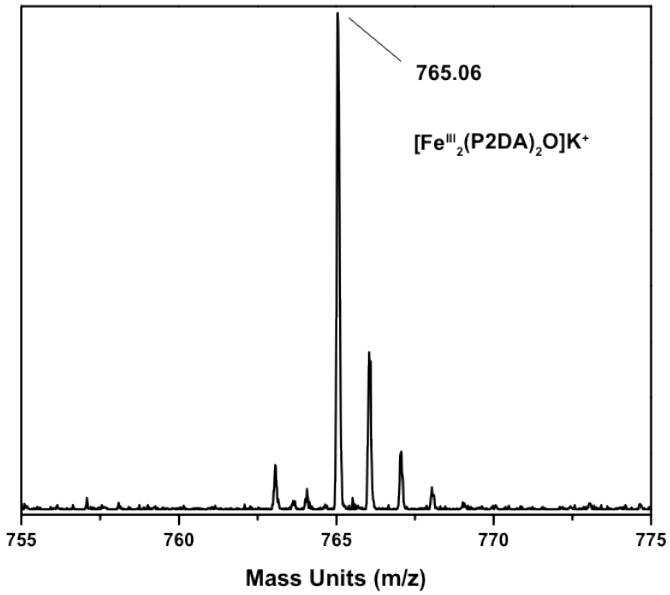

Figure S6. ESI-MS spectrum of the post reaction solution from the reaction between **3(a)** and $NaIO_4$.

This journal is © The Royal Society of Chemistry 2012

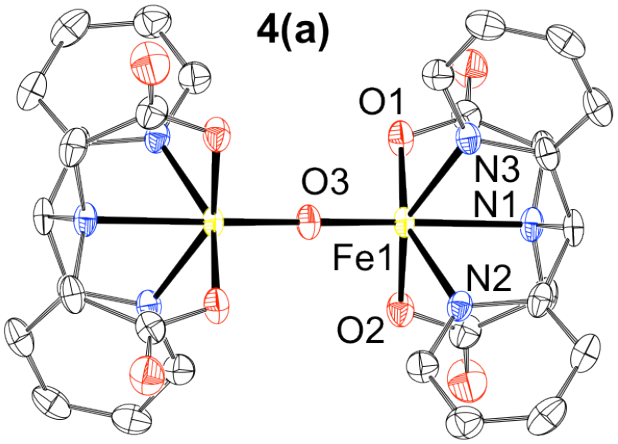

Figure S7. ORTEP plot of complex **4(a)** (50% probability level). Hydrogen atoms and solvent molecules were omitted for clarity.

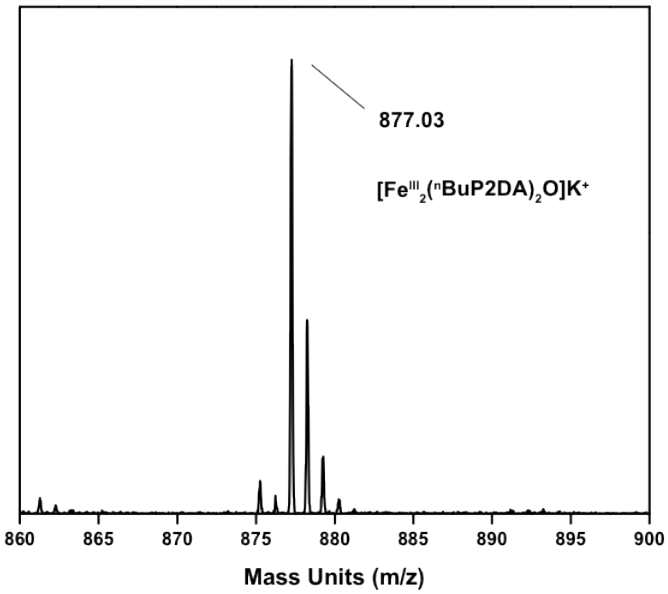

Figure S8. ESI-MS spectrum of the post reaction solution from the reaction between **3(b)-Cl** and ^{S}ArIO.

This journal is © The Royal Society of Chemistry 2012

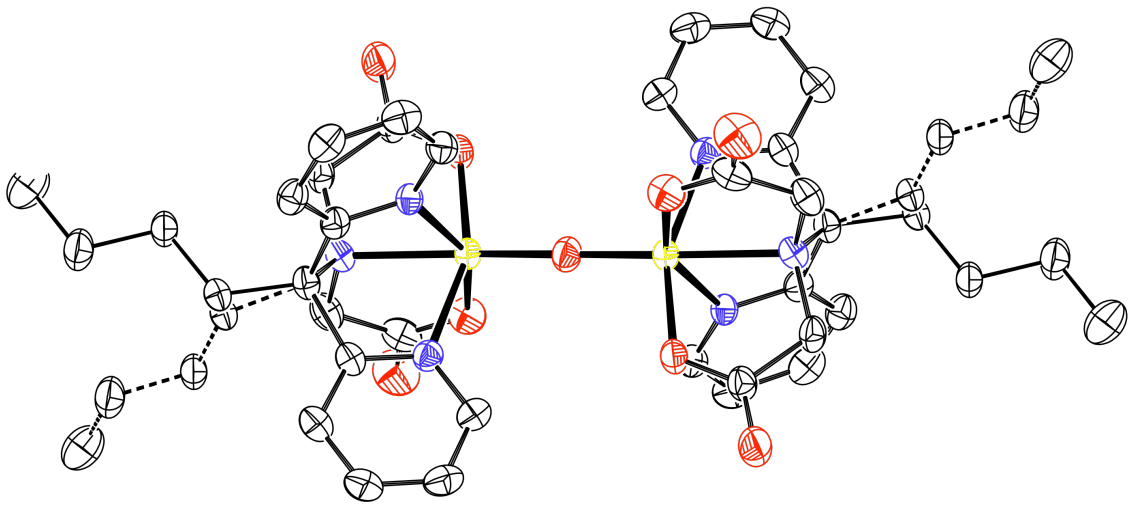

Figure S9. ORTEP plot of complex **4(b)** (50% probability level). Hydrogen atoms and solvent molecules were omitted for clarity.

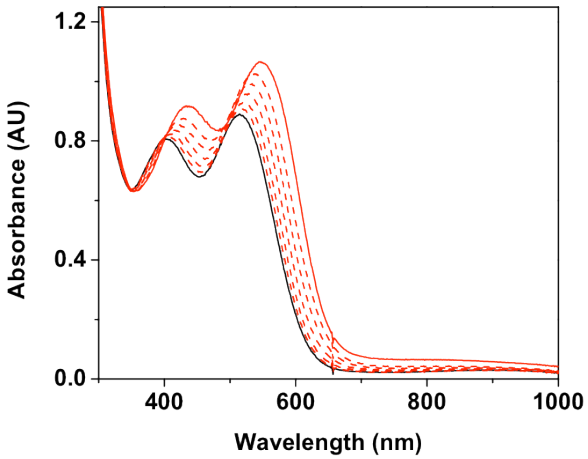

Figure S10. UV-vis absorption spectra depicting the reaction between **3(b)-Cl** (red trace) and ($^{n}Bu_4N$)OH yielding **3(b)-OH** (black trace).

This journal is © The Royal Society of Chemistry 2012

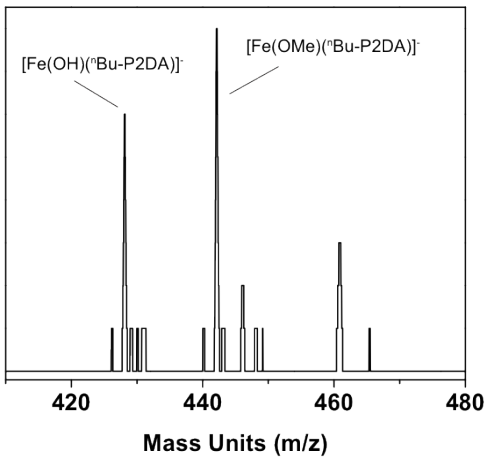

Figure S11. ESI-MS of **3(b)-OH** in negative mode.

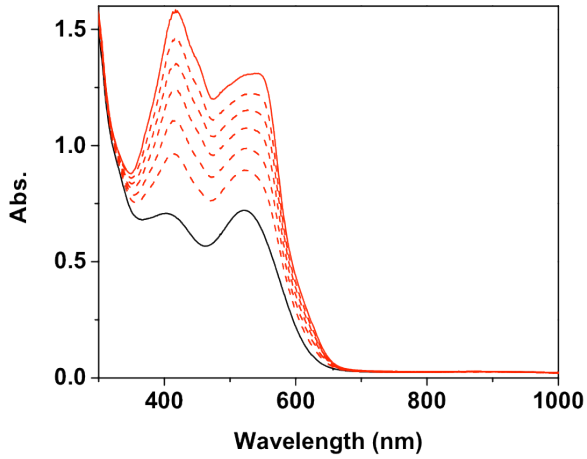

Figure S12. UV-vis absorption spectra depicting the reaction between **3(b)-Cl** (black trace) and pyridine yielding **3(b)-Py** (red trace).

This journal is © The Royal Society of Chemistry 2012

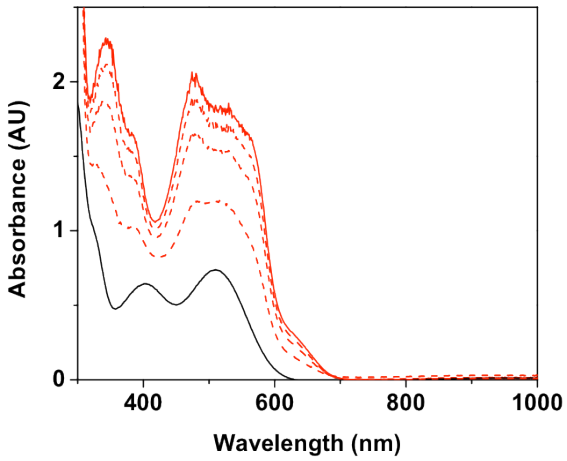

Figure S13. UV-vis absorption spectra depicting the reaction between **3(b)-Cl** (black trace) and 4-dimethylaminopyridine yielding **3(b)-DMAP** (red trace).

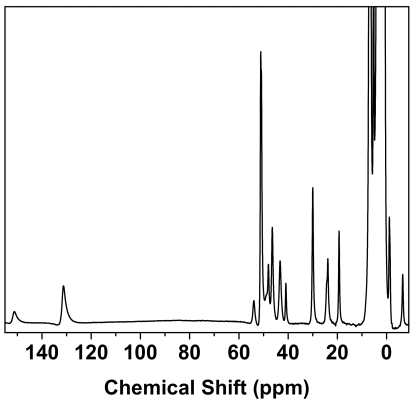

Figure S14. ^{1}H NMR spectrum of **3(b)-Me$_2$Im**

This journal is © The Royal Society of Chemistry 2012

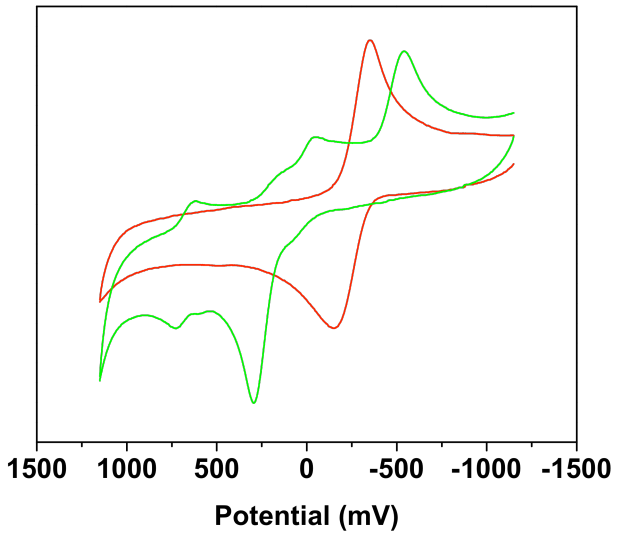

Figure S15. Cyclic voltammagrams of **3(b)-Cl** (red) and **3(b)-Me_2Im** (green), scanning from negative to positive potential.

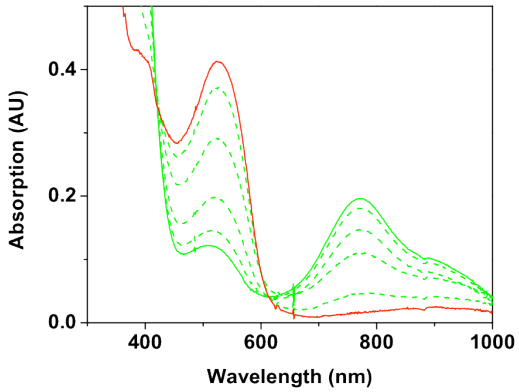

Figure S16. UV-vis analysis of the reaction between **3(b)-Me_2Im** (red trace) and three equiv. ^{s}ArIO at -95 °C in CH_2Cl_2 (1.0 mmol/L) yielding oxoiron(IV) complex **5(b)** (green trace).

This journal is © The Royal Society of Chemistry 2012

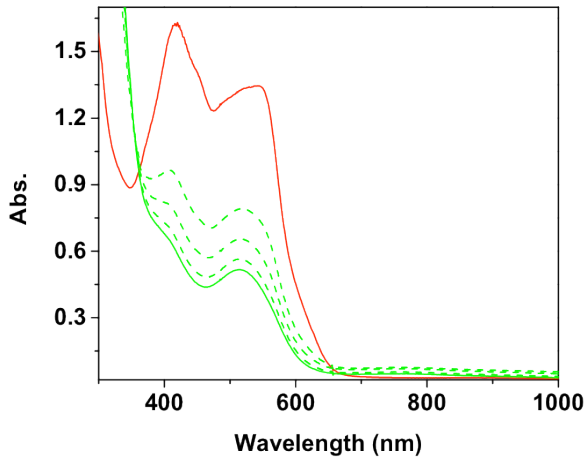

Figure S17. UV-vis absorption spectra depicting the reaction between **3(b)-Py** (red trace) and ^{s}ArIO yielding **5(b)** in 5% yield (green trace).

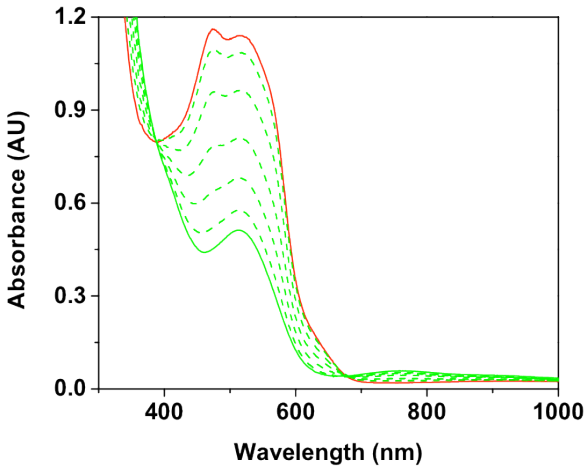

Figure S18. UV-vis absorption spectra depicting the reaction between **3(b)-MeIm** (red trace) and ^{s}ArIO yielding **5(b)** in 40% yield (green trace).

This journal is © The Royal Society of Chemistry 2012

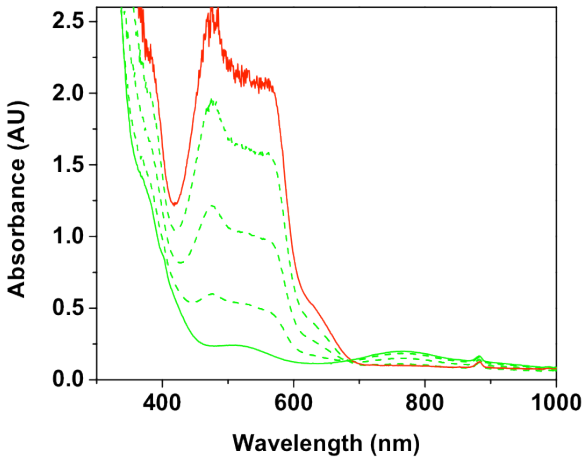

Figure S19. UV-vis absorption spectra depicting the reaction between **3(b)-DMAP** (red trace) and ^{s}ArIO yielding **5(b)** in 75% yield (green trace).

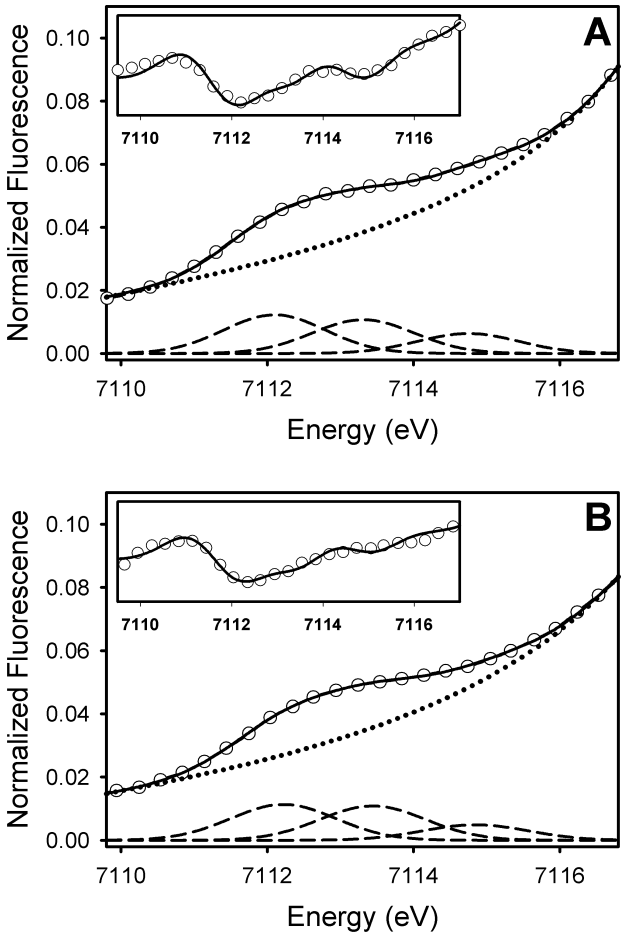

This journal is © The Royal Society of Chemistry 2012

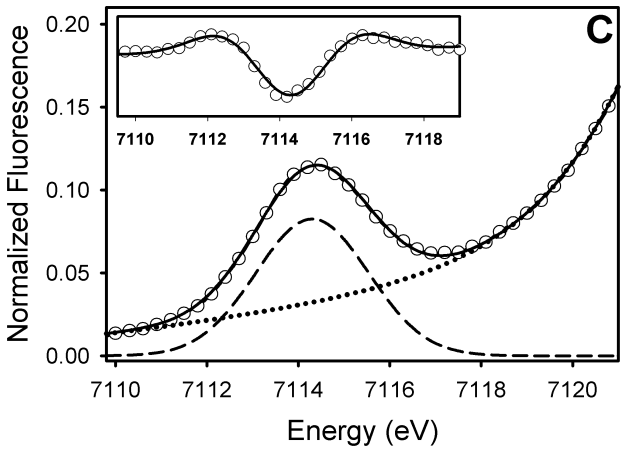

Figure S20. Pre-edge fit for **3(b)-Cl** (A), **3(b)-Me$_2$Im** (B), and **5b** (C). Insets: second derivative spectra and fit.Data points are displayed with (○), fits with (□□), pre-edge peaks with (---), and background with (·····).

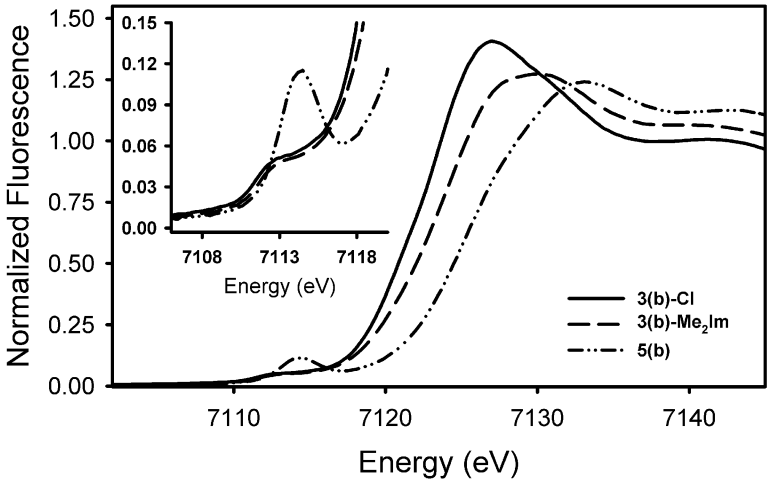

Figure S21. XANES spectra of **3(b)-Cl** (□□), **3(b)-Me$_2$Im** (---), and **5(b)** (–··)

This journal is © The Royal Society of Chemistry 2012

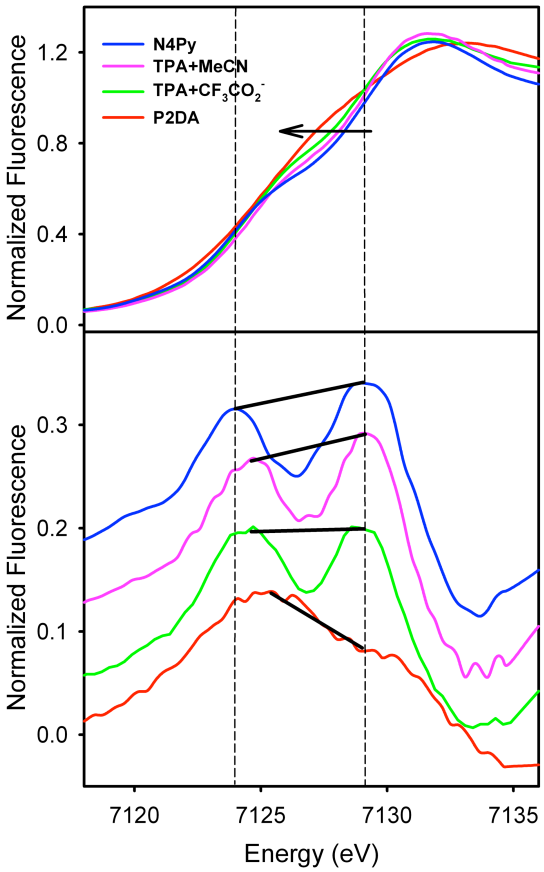

Figure S22. Edge features of **5(b)** (90%) (red), $[Fe^{IV}(O)(TPA)(O_2CCF_3)]^+$ (75%)[19] (green), $[Fe^{IV}(O)(TPA)(NCCH_3)]^{2+}$ (80%)[19, 20] (pink), and $[Fe^{IV}(O)(N4Py)]^{2+}$ (80%) (blue).[20]

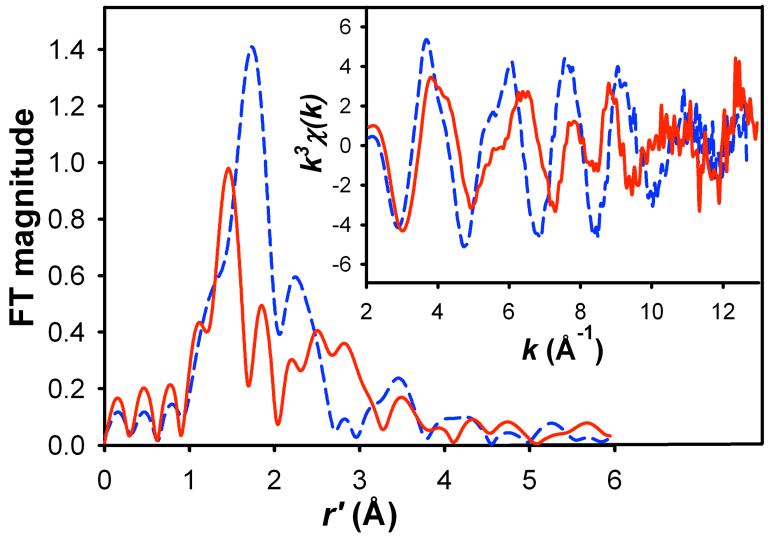

Figure S23. Comparison of EXAFS data of **3(b)-Cl** (□□) and **3(b)-Me$_2$Im** (---)

This journal is © The Royal Society of Chemistry 2012

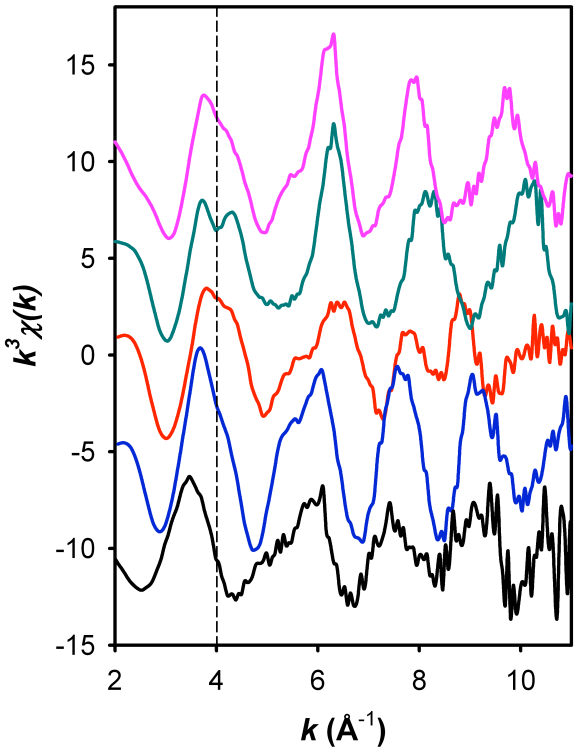

Figure S24. Comparison of EXAFS data of **3(b)-Cl** (blue), **3(b)-Me$_2$Im** (red), [Fe^{II}(TMC)(OTf)]$^+$ (black), [Fe$_2^{II}$(N-Et-HPTB)(O$_2$P(Ph)$_2$)], and [Fe^{II}(Tp')(OBz)].

Electronic Supplementary Material (ESI) for Chemical Science
This journal is © The Royal Society of Chemistry 2012

Table S2. XANES parameters for **3(b)-Cl**, **3(b)-Me_2Im**, **5(b)**, and related oxoiron(IV) complexes

Compound	Pre-edge peak energy (eV)	Peak width at half-height	Peak area	Total peak intensity
3(b)-Cl	7112.1(1)	0.81(3)	2.0(2)	4.9(2)
	7113.3(1)		1.8(1)	
	7114.7(1)		1.1(0)	
3(b)-Me_2Im	7112.3(1)	0.81(3)	1.9(1)	4.3(1)
	7113.5(1)		1.7(0)	
	7114.8(1)		0.8(0)	
5(b)	7114.3(0)	1.44(2)		23.9(5)
$[Fe^{IV}(O)(N4Py)]^{2+}$ (59)	7114.3	1.26(3)		25.2(5)
$[Fe^{IV}(O)(TPA)(NCCH_3)]^{2+}$ (31)	7114.4			26.7
$[Fe^{IV}(O)(TPA)(O_2CCF_3)]^{+}$ (31)	7114.6			25.4

Electronic Supplementary Material (ESI) for Chemical Science
This journal is © The Royal Society of Chemistry 2012

Table S3. EXAFS fitting results for **3(b)-Cl** and **3(b)-Me$_2$Im**. Best fits are shown in bold.

Fit	Fe-O/N			Fe-N/O			Fe-Cl			Fe-C				
#	N	R	σ^2	N	R	σ^2	N	R	σ^2	N	R	σ^2	*F*	*F'*
3(b)-Cl														
1	6	2.17	5.7										84	0.0738
2	5	2.14	3.9	1	2.25	-2.2							75	0.0810
3	4	2.13	2.5	2	2.24	-0.6							76	0.0828
4	5	2.17	8.0				1	2.31	4.8				72	0.0783
5	5	2.16	4.5							6	2.97	8.8	58	0.0635
6	5	2.12	4.9	1	2.22	-2.3				6	2.96	8.2	54	0.0760
7	**5**	**2.15**	**8.7**				**1**	**2.31**	**4.1**	**6**	**2.94**	**7.7**	**15**	**0.0210**
3(b)-Me$_2$Im														
8	6	2.01	22.7										130	0.0966
9	5	2.02	19.1				1	2.64	13.9				118	0.1049
10	2	1.96	2.5	3	2.16	4.6	1	2.67	13.4				66	0.0729
11	2	1.95	1.9	3	2.14	4.0							81	0.0721
12	**2**	**1.95**	**2.4**	**3**	**2.14**	**5.4**				**4** **2**	**2.96** **3.34**	**3.1** **1.0**	**11**	**0.0159**

σ^2 = respective Debye-Waller factor in units of 10^{-3} Å^2. Scale factor S_0^2 = 0.9. GOF = goodness of fit calculated as $F = \sqrt{\sum k^6(\ddot{O}_{exp} - \ddot{O}_{cal})^2}$. $F' = F^2/N.\nu$, where $\nu = n_{idp} - n_{var}$, N is the number of data points, n_{idp} is the number of independent points, and n_{var} is the number of variables used in each optimization step. F' is used to indicate the improvement of fit upon the addition of a shell.[64] **3(b)-Cl**: k range = 2 – 12.7 Å^{-1}, resolution ~ 0.14 Å, back transform range 0.9-3.0 Å, N = 107, n_{idp} = 13.7. **3(b)-Me$_2$Im** : k range = 2 – 13 Å^{-1}, resolution ~ 0.14 Å, back transform range 0.9-3.1 Å, N = 111, n_{idp} = 15.1.

Table S4. EXAFS fitting results for **3(b)-Cl** unfiltered data. Best fits are shown in bold.

	Fe-O/N			Fe-N/O			Fe-Cl			Fe-C			
Fit#	**N**	**R**	**σ^2**	**N**	**R**	**σ^2**	**N**	**R**	**σ^2**	**N**	**R**	**σ^2**	**GOF**
1	6	2.14	7.5										0.4568
2	5	2.14	5.9										0.4341
3	4	2.15	4.2										0.4391
4	5	2.15	5.9	1	2.55	-0.7							0.3544
5	4	2.11	8.5	2	2.20	1.5							0.4198
6	4	2.15	4.8	1	2.21	8.7							0.3527
				1	2.55	-0.9							
7	**5**	**2.16**	**9.9**				**1**	**2.290**	**4.1**				**0.3913**
8	4	2.14	7.7	1	2.33	-0.3	1	2.31	0.2				0.3896
9	4	2.13	7.4	2	2.22	1.3				6	2.96	25.5	0.4117
10	5	2.10	8.8	1	2.20	-1.8				6	2.96	8.7	0.3829
11	4	2.13	6.9	1	2.52	2.4	1	2.32	6.8	6	2.95	8.3	0.2673
12	**2**	**2.08**	**3.6**	**3**	**2.23**	**4.7**	**1**	**2.30**	**3.2**	**6**	**2.95**	**7.8**	**0.2766**
13	**5**	**2.15**	**8.8**				**1**	**2.31**	**3.9**	**6**	**2.94**	**7.8**	**0.2740**

k range = 2 – 12.7 Å^{-1}, resolution ~ 0.15 Å. N = coordination number. R = distance (Å). σ^2 = respective Debye-Waller factor in unit of 10^{-3} Å^2. Scale factor $S_0^2 = 0.9$. GOF = goodness of fit calculated as $F = \sqrt{\sum k^6(\chi_{exp} - \chi_{cal})^2 / \sum k^6 \chi_{exp}^2}$.

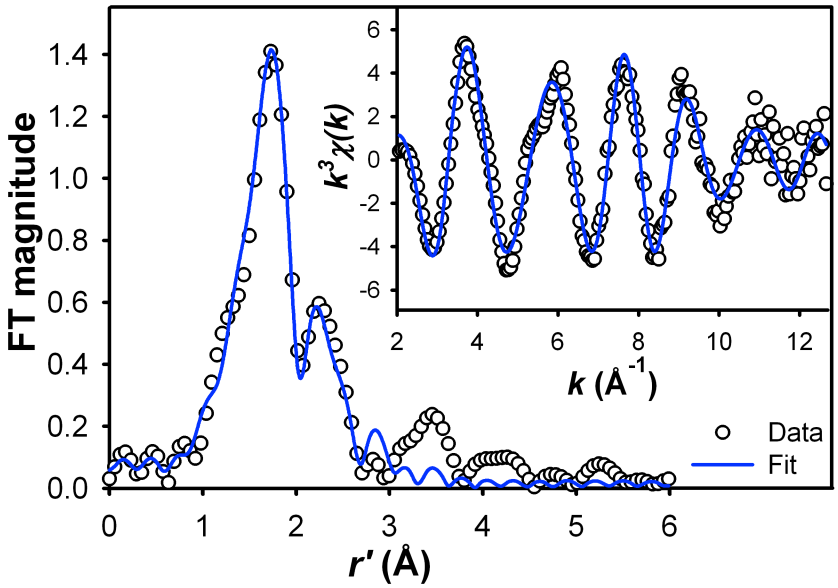

Figure S25. Representative best fit to **3(b)-Cl** unfiltered data (Fit 13, Table S1).

Electronic Supplementary Material (ESI) for Chemical Science
This journal is © The Royal Society of Chemistry 2012

Table S5. EXAFS fitting results for **3(b)-Cl** filtered data. Best fits are shown in bold.

Fit	**Fe-O/N**			**Fe-N/O**			**Fe-Cl**			**Fe-C**				
#	**N**	**R**	**σ^2**	**N**	**R**	**σ^2**	**N**	**R**	**σ^2**	**N**	**R**	**σ^2**	***F***	***F'***
1	6	2.17	5.7										84	0.0738
2	5	2.17	4.3										81	0.0713
3	4	2.17	3.0										98	0.0861
4	5	2.18	4.3	1	2.57	-0.8							51	0.0550
5	4	2.19	3.0	2	2.58	2.4							80	0.0865
6	3	2.20	1.7	3	2.58	4.9							153	0.1659
7	3	2.11	1.4	3	2.23	0.2							76	0.0824
8	4	2.13	2.5	2	2.24	-0.6							76	0.0828
9	5	2.14	3.9	1	2.25	-2.2							75	0.0810
10	2	2.09	2.8	3	2.26	4.9	1	2.31	2.1				73	0.1038
11	**5**	**2.17**	**8.0**				**1**	**2.31**	**4.8**				**72**	**0.0783**
12	3	2.17	1.2	3	2.59	3.9				6	2.96	10.3	85	0.1203
13	4	2.16	2.8	2	2.57	1.4				6	2.96	10.6	27	0.0379
14	5	2.16	4.1	1	2.56	-1.6				6	2.97	9.7	13	0.0184
15	3	2.09	1.5	3	2.21	-0.1				6	2.96	8.5	53	0.0750
16	4	2.10	2.6	2	2.22	-1.3				6	2.96	7.9	53	0.0744
17	5	2.12	4.9	1	2.22	-2.3				6	2.96	8.2	54	0.0760
18	5	2.16	4.5							6	2.97	8.8	58	0.0635
19	2	2.08	2.3	3	2.25	4.2	1	2.30	2.0	6	2.96	7.8	16	0.0322
20	**5**	**2.15**	**8.7**				**1**	**2.31**	**4.1**	**6**	**2.94**	**7.7**	**15**	**0.0210**

k range = 2 – 12.7 Å^{-1}, resolution ~ 0.15 Å, back transform range 0.9-3.0 Å. σ^2 = respective Debye-Waller factor in unit of 10^{-3} Å^2. Scale factor $S_0^2 = 0.9$. GOF = goodness of fit calculated as $F = \sqrt{\sum k^6(\chi_{exp} - \chi_{cal})^2}$. $F' = F^2/N.\nu$, where $\nu = n_{idp} - n_{var}$, $N = 107$ is the number of data point, $n_{idp} = 13.7$ is the number of independent points, and n_{var} is the number of variables used in each optimization step. F' is used to indicate the improvement of fit upon the addition of a shell.

Table S6. EXAFS fitting result for **3(b)-Me_2Im** unfiltered data. Best fits are shown in bold.

	Fe-O/N			Fe-N/O			Fe-N/Cl			Fe-C			
Fit#	**N**	**R**	**σ^2**	**N**	**R**	**σ^2**	**N**	**R**	**σ^2**	**N**	**R**	**σ^2**	**GOF**
1	6	2.03	20.0										0.6746
2	5	2.02	16.7										0.6731
3	4	2.02	13.7										0.6843
4	5	1.97	12.3	1	2.19	-1.2							0.6012
5	4	1.96	8.1	2	2.18	1.7							0.5904
6	3	1.95	4.7	3	2.16	4.2							0.5759
7	**2**	**1.94**	**2.3**	**4**	**2.14**	**7.6**							**0.5574**
8	1	1.93	-0.3	5	2.19	13.3							0.5432
9	2	1.95	1.8	3	2.14	4.2							0.5607
10	**2**	**1.95**	**1.4**	**3**	**2.14**	**3.0**	**1**	**2.30**	**4.3**				**0.5462**
11	2	1.95	2.0	3	2.15	4.3	1Cl	2.64	15.4				0.5246
12	**2**	**1.95**	**1.4**	**3**	**2.14**	**2.9**	**1**	**2.31**	**3.8**	**4**	**2.97**	**3.3**	**0.3487**
										2	**3.35**	**3.3**	
13	**2**	**1.94**	**2.3**	**4**	**2.14**	**8.2**				**4**	**2.96**	**2.5**	**0.3594**
										2	**3.35**	**0.9**	
14	**2**	**1.94**	**2.0**	**3**	**2.14**	**5.1**				**4**	**2.95**	**2.6**	**0.3520**
										2	**3.35**	**0.7**	

k range = 2 – 13Å^{-1}, resolution ~ 0.14 Å. N = coordination number. R = distance (Å). σ^2 = respective Debye-Waller factor in unit of 10^{-3} Å^2. Scale factor $S_0^2 = 0.9$. GOF = goodness of fit calculated as $F = \sqrt{\sum k^6(\chi_{exp} - \chi_{cal})^2 / \sum k^6 \chi_{exp}^2}$.

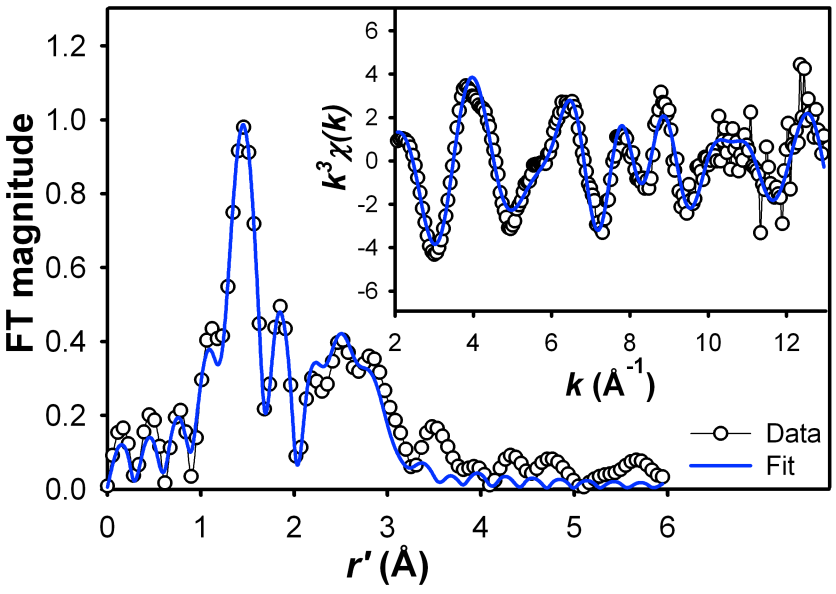

Figure S26. Representative best fit to **3(b)-Me_2Im** unfiltered data (Fit 14, Table S5).

This journal is © The Royal Society of Chemistry 2012

Table S7. EXAFS fitting result for **3(b)-Me_2Im** filtered data. Best fits are shown in bold.

Fit	Fe-O/N			Fe-N/O			Fe-N/Cl			Fe-C				
#	N	R	σ^2	N	R	σ^2	N	R	σ^2	N	R	σ^2	*F*	*F'*
1	6	2.01	22.7										130	0.0966
2	5	2.01	19.5										127	0.0949
3	4	1.99	15.2										129	0.0961
4	**2**	**1.94**	**3.2**	**4**	**2.15**	**8.2**							**80**	**0.0712**
5	1	1.93	0.3	5	2.13	14.2							75	0.0671
6	**2**	**1.95**	**1.9**	**3**	**2.14**	**4.0**							**81**	**0.0721**
7	3	1.97	5.6	2	2.18	1.6							88	0.0781
8	2	1.96	2.3	2	2.16	1.5							90	0.0805
9	1	1.93	-0.4	4	2.12	9.8							72	0.0641
10	1	1.94	-0.9	3	2.12	6.4							78	0.0698
11	3	1.97	6.4	1	2.18	-1.5							90	0.0800
12	**2**	**1.96**	**1.1**	**3**	**2.15**	**1.7**	**1**	**2.32**	**0.8**				**75**	**0.0830**
13	2	1.96	2.5	3	2.16	4.6	1Cl	2.67	13.4				66	0.0729
14	2	1.96	2.7	2	2.15	2.1	1Cl	2.61	18.8				74	0.0825
15	2	1.94	2.9	4	2.14	9.0				4	2.96	3.1	27	0.0298
16	2	1.94	2.4	3	2.14	5.6				4	2.96	3.3	22	0.0250
17	2	1.95	2.0	3	2.14	4.2	1	2.31	7.7	4	2.97	3.2	25	0.0363
18	**2**	**1.94**	**3.1**	**4**	**2.14**	**8.8**				**4**	**2.96**	**3.1**	**14**	**0.0209**
										2	**3.33**	**1.1**		
19	**2**	**1.95**	**2.4**	**3**	**2.14**	**5.4**				**4**	**2.96**	**3.1**	**11**	**0.0159**
										2	**3.34**	**1.0**		
20	2	1.95	2.0	3	2.14	3.8	1	2.31	5.5	4	2.97	3.3	11	0.0243
										2	3.34	1.1		

k range = 2 – 13 $Å^{-1}$, resolution ~ 0.14 Å, back transform range 0.9-3.1 Å. σ^2 = respective Debye-Waller factor in unit of 10^{-3} $Å^2$. Scale factor $S_0^2 = 0.9$. GOF = goodness of fit calculated as $F = \sqrt{\sum k^6(\chi_{exp} - \chi_{cal})^2}$. $F' = F^2/N.\nu$, where $\nu = n_{idp} - n_{var}$, $N = 111$ is the number of data point, $n_{idp} = 15.1$ is the number of independent points, and n_{var} is the number of variables used in each optimization step. F' is used to indicate the improvement of fit upon the addition of a shell.

This journal is © The Royal Society of Chemistry 2012

Table S8. EXAFS fitting results for **5(b)**. Best fits are shown in bold.

	Fe-O			Fe-O/N			Fe-N			Fe-C			
Fit#	**N**	**R**	**σ^2**	**N**	**R**	**σ^2**	**N**	**R**	**σ^2**	**N**	**R**	**σ^2**	**GOF**
1				6	1.97	17.5							0.7913
2				5	1.96	12.1							0.7408
3				4	1.96	8.3							0.6784
4				5	1.98	10.9	1	2.25	3.1				0.7017
5				4	1.98	7.9	2	2.26	11.0				0.6486
6				3	1.98	5.1	3	2.24	19.3				0.6095
7				4	1.98	7.6	1	2.23	2.9				0.6464
8				3	1.98	5.0	2	2.22	13.4				0.6050
9	0.9	1.66	2.8	5	1.97	9.1							0.5324
10	0.9	1.66	4.1	4	1.97	6.5							0.5355
11	0.9	1.68	5.2	3	1.96	2.5	2	2.11	5.0				0.5076
12	0.9	1.69	5.6	2	1.95	1.0	3	2.08	7.9				0.5062
13	0.9	1.68	4.8	4	1.97	4.4	1	2.16	0.9				0.5097
14				5	1.99	9.6				2	2.80	1.1	0.6709
										3	2.99	0.4	
15				4	2.00	5.9	1	2.24	2.4	2	2.78	2.5	0.5828
										3	2.99	1.2	
16				4	1.99	6.8				2	2.78	1.4	0.5962
										3	2.99	0.9	
17	0.9	1.66	2.9	5	1.97	8.9				2	2.78	3.1	0.4821
										3	2.98	2.2	
18	**0.9**	**1.67**	**4.3**	**4**	**1.97**	**5.9**	**1**	**2.14**	**8.5**	**2**	**2.78**	**3.0**	**0.4640**
										3	**2.99**	**2.2**	
19	**0.9**	**1.66**	**4.6**	**4**	**1.97**	**6.5**				**2**	**2.78**	**2.7**	**0.4663**
										3	**2.98**	**1.9**	

k range = 2 – 12.4 Å^{-1}, resolution ~ 0.15 Å. N = coordination number. R = distance (Å). σ^2 = respective Debye-Waller factor in unit of 10^{-3} Å^2. Scale factor $S_0^2 = 0.9$. GOF = goodness of fit calculated as $F = \sqrt{\sum k^6(\chi_{exp} - \chi_{cal})^2 / \sum k^6 \chi_{exp}^2}$.

This journal is © The Royal Society of Chemistry 2012

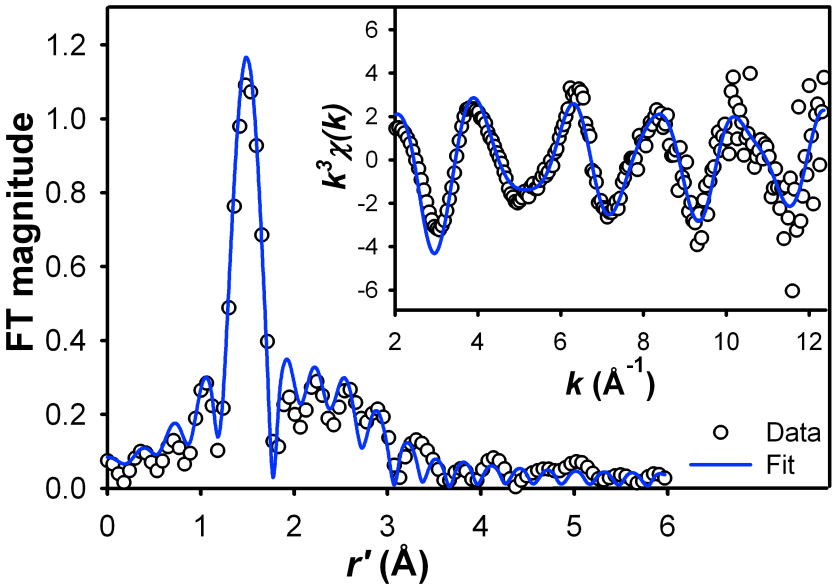

Figure S27. Best fit to **5(b)** unfiltered data (Fit 19, Table S7)

This journal is © The Royal Society of Chemistry 2012

Table S9. EXAFS fitting results for **5(b)** filtered data. Best fits are shown in bold.

Fit	Fe=O			Fe-O/N			Fe-N/O			Fe---C				
#	N	R	σ^2	N	R	σ^2	N	R	σ^2	N	R	σ^2	*F*	*F'*
1				6	1.99	13.8							142	0.1169
2				5	1.99	10.0							111	0.0911
3				4	1.99	7.0							82	0.0670
4				3	2.00	4.3	3	2.25	25.1				70	0.0690
5				4	2.00	6.8	2	2.29	13.7				82	0.0814
6				5	2.00	9.1	1	2.26	2.7				102	0.1012
7				4	2.00	6.0	1	2.23	1.9				75	0.0740
8				3	2.00	2.6	1	2.18	0.2				52	0.0519
9				3	2.00	4.0	2	2.22	13.4				63	0.0627
10	**0.9**	**1.67**	**5.5**	**4**	**1.98**	**5.0**	**1**	**2.17**	**3.0**				**32**	**0.0404**
11	0.9	1.69	8.9	3	1.97	1.4	1	2.14	-1.0				29	0.0361
12	0.9	1.67	6.1	3	1.96	3.3	2	2.11	7.8				31	0.0392
13	0.9	1.68	6.8	2	1.96	1.9	3	2.07	11.8				31	0.0386
14	**0.9**	**1.66**	**4.8**	**4**	**1.97**	**6.6**							**39**	**0.0383**
15	0.9	1.66	3.1	5	1.97	9.1							40	0.0393
				5	1.99	9.8				2	2.81	1.9	98	0.1223
										3	3.00	1.0		
16				4	2.00	6.3	1	2.25	3.8	2	2.79	2.5	60	0.1011
										3	3.00	1.4		
17	0.9	1.65	3.2	5	1.97	9.2				2	2.78	3.4	23	0.0388
										3	2.99	2.8		
18	**0.9**	**1.66**	**5.0**	**4**	**1.98**	**6.6**				**2**	**2.78**	**3.2**	**17**	**0.0295**
										3	**2.99**	**2.4**		
19	0.9	1.66	5.4	4	1.97	5.7	1	2.17	8.4	2	2.78	4.4	18	0.0468
										3	2.99	2.7		

k range = 2 – 12.4 Å^{-1}, resolution ~ 0.15 Å, back transform range 0.85-3.1 Å. σ^2 = respective Debye-Waller factor in unit of 10^{-3} Å^2. Scale factor S_0^2 = 0.9. GOF = goodness of fit calculated as $F = \sqrt{\sum k^6(\chi_{exp} - \chi_{cal})^2}$. $F' = F^2/N.\nu$, where $\nu = n_{idp} - n_{var}$, $N = 104$ is the number of data point, $n_{idp} = 14.7$ is the number of independent points, and n_{var} is the number of variables used in each optimization step. F' is used to indicate the improvement of fit upon the addition of a shell.

This journal is © The Royal Society of Chemistry 2012

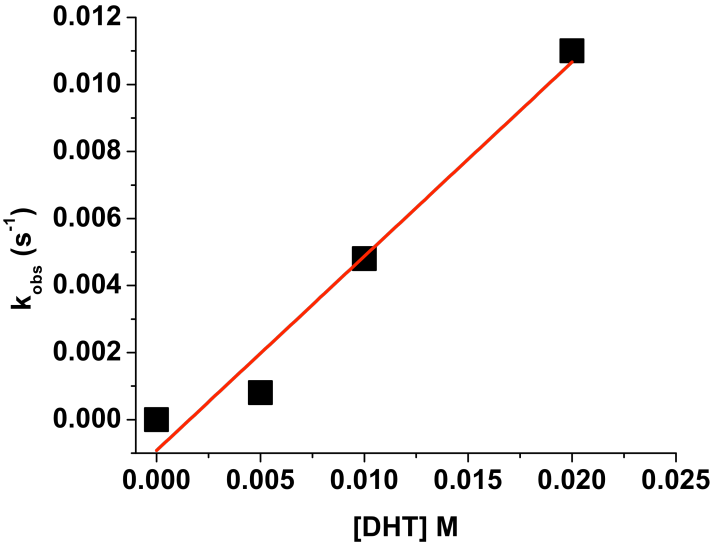

Figure S28. Plot of the pseudo-first-order rate constants (k_{obs} (s^{-1})) obtained for **5(b)** against DHT concentration to determine second order rate constant (k_2 ($M^{-1}s^{-1}$)).

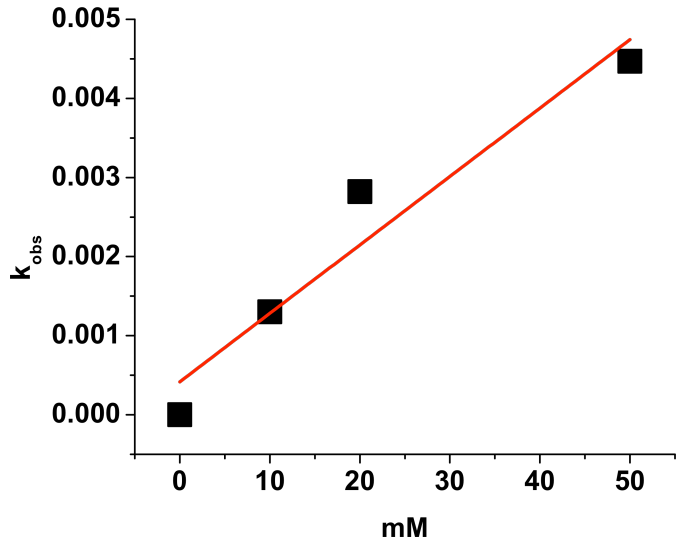

Figure S29. Plot of the pseudo-first-order rate constants (k_{obs} (s^{-1})) obtained for $[Fe^{IV}(O)(N4Py)]^{2+}$ against DHT concentration to determine second order rate constant (k_2 ($M^{-1}s^{-1}$)).

This journal is © The Royal Society of Chemistry 2012

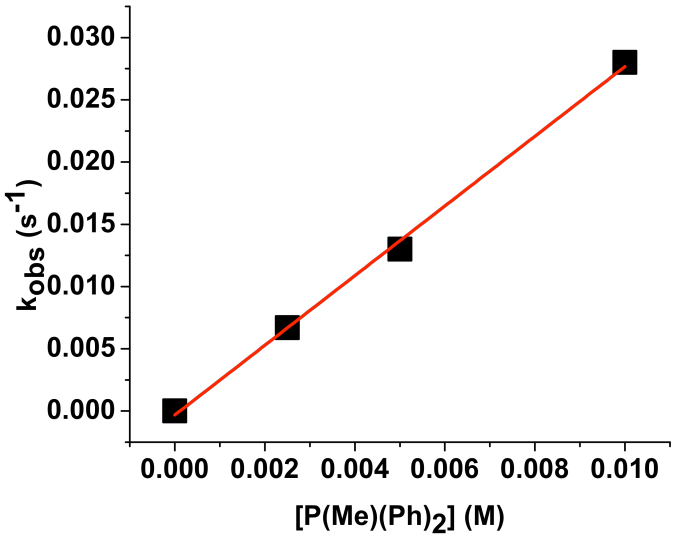

Figure S30. Plot of the pseudo-first-order rate constants (k_{obs} (s^{-1})) obtained for **5(b)** against $P(Me)(Ph)_2$ concentration to determine second order rate constant (k_2 ($M^{-1}s^{-1}$)).

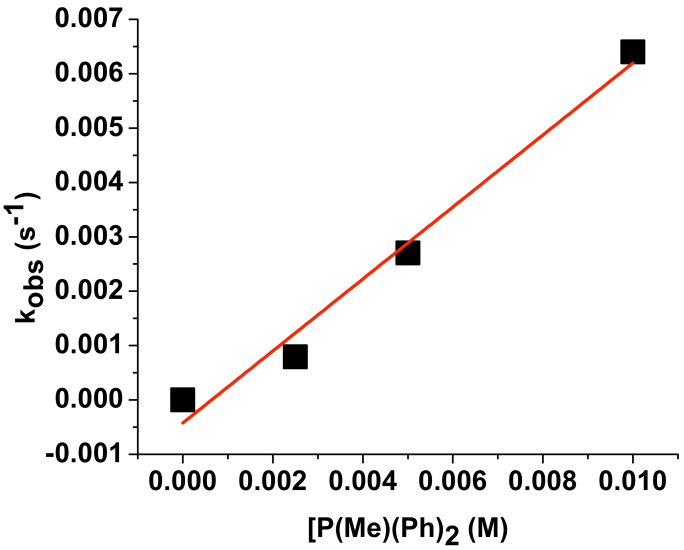

Figure S31. Plot of the pseudo-first-order rate constants (k_{obs} (s^{-1})) obtained for $[Fe^{IV}(O)(N4Py)]^{2+}$ against $P(Me)(Ph)_2$ concentration to determine second order rate constant (k_2 ($M^{-1}s^{-1}$)).

This journal is © The Royal Society of Chemistry 2012

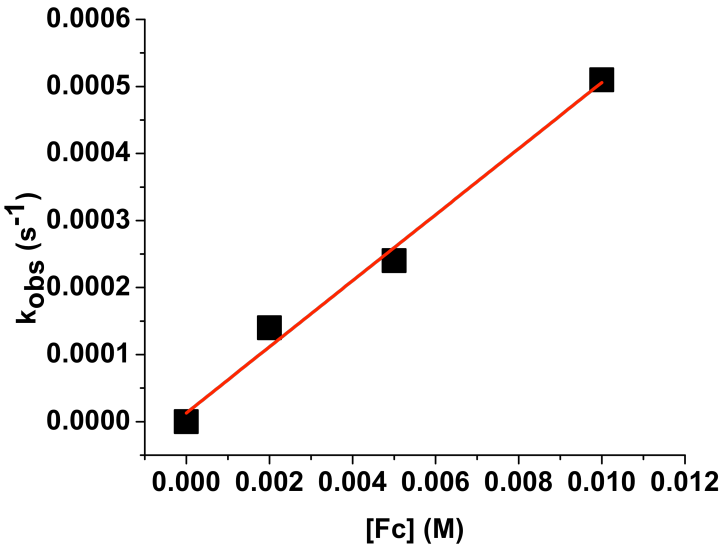

Figure S32. Plot of the pseudo-first-order rate constants (k_{obs} (s^{-1})) obtained for **5(b)** against Fc concentration to determine second order rate constant (k_2 ($M^{-1}s^{-1}$)).

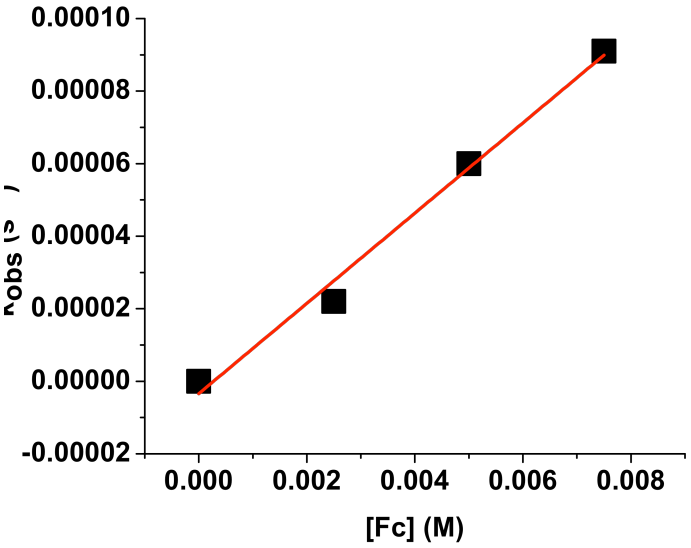

Figure S33. Plot of the pseudo-first-order rate constants (k_{obs} (s^{-1})) obtained for $[Fe^{IV}(O)(N4Py)]^{2+}$ against Fc concentration to determine second order rate constant (k_2 ($M^{-1}s^{-1}$)).

This journal is © The Royal Society of Chemistry 2012

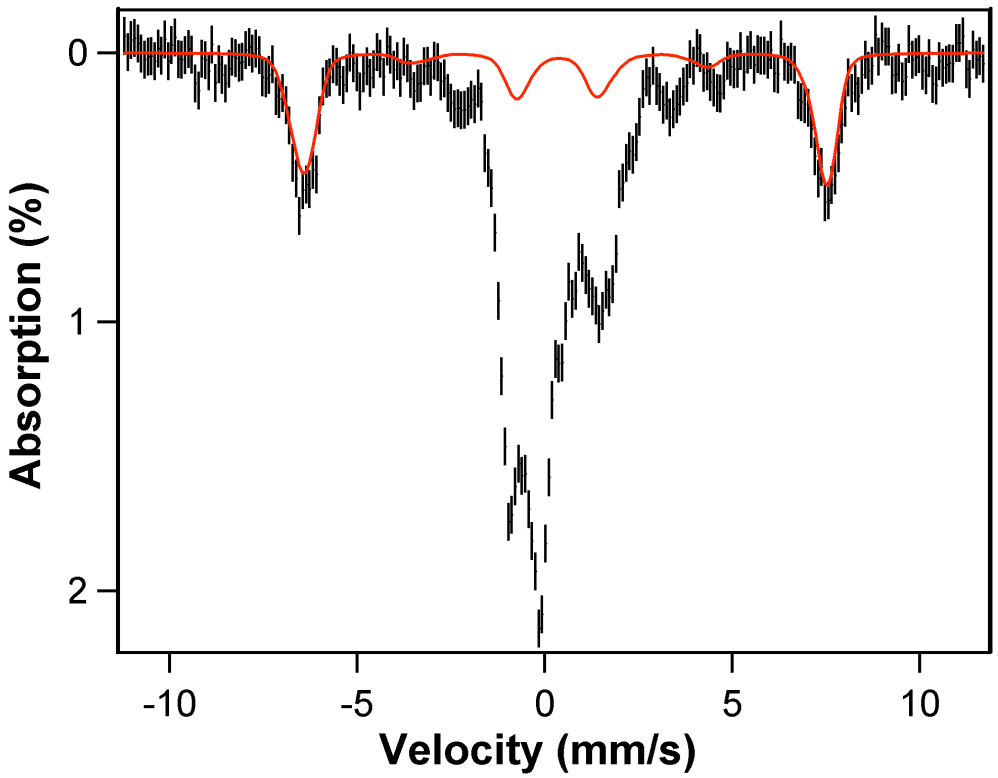

Figure S34. 4.2 K Mössbauer spectrum of the sample containing complex **5(b)** measured in frozen Methanol solution under 8.0 T parallel applied field. The red curve is the simulation of mononuclear high spin ferric impurity, representing 20% total Fe in the sample.

This journal is © The Royal Society of Chemistry 2012

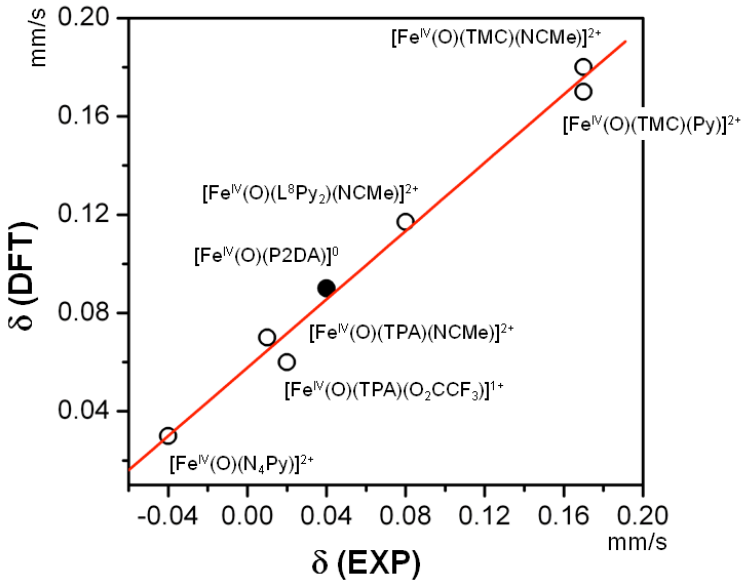

Figure S35. Correlation between DFT calculated and experimental determined isomer shifts for a series of $[Fe^{IV}(O)(L)]$ complexes. The correlation coefficient R^2 is 0.99. Complex **5(b)** is indicated with a solid dot (see the last section in the supporting information for the discussion of DFT calculated isomer shift of $[Fe^{IV}(O)(TPA)(O_2CCF_3)]^+$).

This journal is © The Royal Society of Chemistry 2012

Table S10. Comparison of DFT calculated contributions to the total energies of the $S = 2$ exited state relative to the $S = 1$ ground state for complexes **5(b)** and $[Fe^{IV}(O)(N4Py)]^{2+}$.[a]

	$\Delta E_{electronic}$	ΔE_{ZPE}	$\Delta E_{thermal}$	$\Delta E_{enthalpy}$	$\Delta E_{entropy}$	$\Delta E_{solvent}$	ΔE_{total}
$[Fe^{IV}(O)(N4Py)]^{2+}$ ($S = 2$)[b]	2897.5	-399.7	131.0	0	-412.8	244.8	2460.7
5(b) (S=2)[b]	193.4	-276.4	109.2	0.2	-357.8	972.8	641.5

[a] Energies are in wavenumbers; all the calculations were performed based on optimized geometries for $S = 1$ and $S = 2$ spin states obtained by the gas-phase calculations; the thermal energies were calculated at -95 ºC. [b] In each term, the energies for the $S = 1$ spin state were taken as the origin of the energy scale.

This journal is © The Royal Society of Chemistry 2012

Table S11. Selected bond lengths and angles from DFT optimized [Fe^{IV}(O)(^{n}Bu-P2DA)] in $S = 1$ and $S = 2$ spin states.[a]

Selected bond lengths (Å) and angles (°)	**Fe^{IV}(O)(^{n}BuP2DA)**	
	S = 1	S = 2
Fe-O	1.64748	1.64002
Fe-N(1)	1.9894	2.18016
Fe-N(2)	1.97843	2.13282
Fe-N(3)	2.11992	2.17896
Fe-O(1)	1.92253	1.97004
Fe-O(2)	1.91935	1.94576
O-Fe-N(1)	95.199	97.413
O-Fe-N(2)	94.750	96.194
O-Fe-O(1)	100.746	103.270
O-Fe-O(2)	99.602	101.638
O-Fe-N(3)	173.248	171.193
N(1)-Fe-N(3)	79.697	75.703
N(2)-Fe-N(3)	80.591	77.314
O(1)-Fe-N(3)	84.079	82.368
O(2)-Fe-N(3)	84.871	83.700
N(1)-Fe-N(2)	86.320	79.525
O(1)-Fe-O(2)	91.746	100.792
O(1)-Fe-N(2)	88.264	85.713
O(2)-Fe-N(1)	89.624	87.133
O(1)-Fe-N(1)	163.530	155.740
O(2)-Fe-N(2)	165.385	158.962

[a] Please refer to Figure 11 for the atom labeling.

Electronic Supplementary Material (ESI) for Chemical Science
This journal is © The Royal Society of Chemistry 2012

Estimate of zero-field splitting D

The zero-field splitting (ZFS) parameters D for the $S = 1$ ground state of complex **5(b)** and $[Fe^{IV}(O)(N4Py)]^{2+}$ are estimated by the second-order perturbation theory treatment of the spin-orbit coupling between the ground state and various excited states within the $S = 1$ spin manifold as well as $S = 2$ and $S = 0$ excited spin manifold.[21, 22] It can be expressed as[21]

$$D = D_{S=0} + D_{S=1} + D_{S=2} \qquad \text{(S1)}$$

$$D_{S=0} = \gamma_{xz}\gamma_{yz}\frac{\zeta^2}{2\Delta_1} + \gamma_{yz}\gamma_{xz}\frac{\zeta^2}{2\Delta_2}$$

$$D_{S=2} = \gamma_{xy}\gamma_{x^2-y^2}\frac{\zeta^2}{3\Delta_3}$$

$$D_{S=1} = \gamma_{xz,yz}\gamma_{z^2}\frac{3\zeta^2}{4\Delta_4} + \gamma_{xy}\gamma_{xz,yz}\frac{\zeta^2}{4\Delta_5} + \gamma_{xz,yz}\gamma_{x^2-y^2}\frac{\zeta^2}{4\Delta_6}$$

Where $D_{S=0}$, $D_{S=1}$, and $D_{S=2}$ represent the contributions to D from the spin-orbit coupling of the ground state $|xy^{\alpha}xy^{\beta}xz^{\alpha}yz^{\alpha}|$ with excited states of $S = 0$, 1, and 2 manifold respectively. The transition energies Δ_i within the $S = 1$ manifold were estimated by using TD-DFT calculations, the transition energies for $S = 0$ and 2 were evaluated by taking the difference of the DFT SCF energies for spin states $S = 0$, 2 and spin state $S = 1$ using the optimized structure for the $S = 1$ state (Table S11 and S12). γ_Γ are covalency factors ($0 \leq \gamma_\Gamma \leq 1$) that measure the 3d character of molecular orbitals, they were estimated from the Mulliken population of the 3d orbitals of iron[21] [] and are listed in Table S13. For the spin-orbit coupling constant, we adopted a value $\zeta \cong 490$ cm^{-1} that is slightly smaller than the free Fe^{IV} ion value $\zeta \cong 510$ cm^{-1}. Contributions from different spin states are listed in Table S11 and S12, and collectively the ZFS parameters D for the $S = 1$ complexes **5(b)** and $[Fe^{IV}(O)(N4Py)]^{2+}$ are $D_{P2DA} = D_{S=0} + D_{S=1} + D_{S=2} = 30.5$ cm^{-1}, and $D_{N4Py} = D_{S=0} + D_{S=1} + D_{S=2} = 23.2$ cm^{-1}, which are consistent with the Mössbauer determined value (Table 4).

This journal is © The Royal Society of Chemistry 2012

Table S12. Excited states and their contributions to zero field splitting parameters D for $[Fe^{IV}(O)(N4Py)]^{2+}$.

Label, i	Spin, *S*	Transition	Δ_i (cm^{-1})	D_S (cm^{-1})
1	0	xz → yz	10614	8.0
2	0	yz → xz	10614	
3	2	xy → x^2-y^2	6210	8.5
4	1	xz,yz → z^2	22422	6.8
5	1	xy → xz,yz	12795	
6	1	xz,yz → x^2-y^2	19125	

Table S13. Excited states and their contributions to zero field splitting parameters D for **5(b)**.

Label, i	Spin, *S*	Transition	Δ_i (cm^{-1})	D_S (cm^{-1})
1	0	xz → yz	10950	7.8
2	0	yz → xz	10950	
3	2	xy → x^2-y^2	3550	15
4	1	xz,yz → z^2	20100	7.7
5	1	xy → xz,yz	11500	
6	1	xz,yz → x^2-y^2	16900	

Table S14. Covalency factors for calculating zero field splitting [a].

d	γ_Γ
xy	0.96
xz	0.59
yz	0.58
x^2-y^2	0.70
z^2	0.59

[a] Covalency factors have been estimated from the Mulliken populations of the iron 3d orbitals. The values for the complex **5(b)** and N4Py differ by a few percent; therefore, the average values over the two complexes are used.

This journal is © The Royal Society of Chemistry 2012

Table S15. DFT calculated atomic orbital contributions to the iron 3d orbitals in the β spin space for complexes **5(b)** and $[Fe^{IV}(O)(N4Py)]^{2+}$.

	5(b)					**$[Fe^{IV}(O)(N4Py)]^{2+}$**		
	Fe	O	nBuP2DA	O_p[a]	O_d[a]	Fe	O	N4Py
z^2	58	20	22	-	-	54	20	26
x^2-y^2	69	0	31	-	-	62	0	38
xz	46	33	21	-	-	53	37	10
yz	43	26	31	-	-	49	39	12
xy	49	0	51	28	18	72	0	28

[a] O_p: the oxygen atoms from the carboxylate ligand directly ligating to the iron; O_d: the distal oxygen atoms from the carboxylate ligands.

This journal is © The Royal Society of Chemistry 2012

Table S16. The TD-DFT calculated vertical transition energies of selected d-d transitions responsible for the near-IR features observed experimentally in various $S = 1$ Fe^{IV}=O complexes.[a]

	TMC-py	TMC/$NCCH_3$	L^8Py_2	**5(b)**	TPA/O_2CCF_3	TPA/$NCCH_3$	N4Py
$xy \rightarrow xz/yz$ [b]	1.52 (<0.1)	1.50 (<0.1)	1.64 (0.1)	1.43 (<0.1)	1.50 (0.1)	1.59 (0.1)	1.59 (<0.1)
$xz/yz \rightarrow x^2\text{-}y^2$ [b]	1.92 (1.6)	2.00 (2.3)	2.05 (2.3)	2.10 (2.9)	2.29 (3.0)	2.31 (3.7)	2.36 (4.1)
$xy \rightarrow x^2\text{-}y^2$	1.14 (<0.1)	1.20 (<0.1)	1.42 (<0.1)	1.29 (<0.1)	1.49 (<0.1)	1.50 (<0.1)	1.65 (<0.1)
Experimental [c]	1.49	1.50	1.57	1.61	1.66	1.71	1.79

[a] Transition energies are given in eV. The numbers in parenthesis are the oscillator strength $\times 10^3$. [b] The two transitions are close in energy, therefore the average value are listed. [c] the experimental value reported here are taken from the peak position of the near-IR feature.

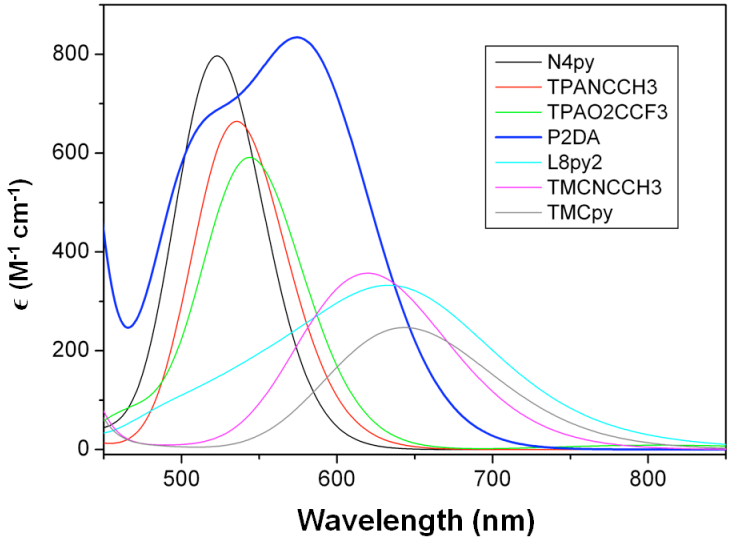

Figure S36. The near-IR region of the TD-DFT calculated electronic absorption spectra of various $S = 1$ Fe^{IV}=O complexes supported by different ligand systems mentioned in this study.

This journal is © The Royal Society of Chemistry 2012

DFT Calculations on $[Fe^{IV}(O)(TPA)(O_2CCF_3)]^+$

In the main text, we have presented electronic parameters of $[Fe^{IV}(O)(TPA)(O_2CCF_3)]^+$ obtained by DFT calculations. Some of the results have been published in[19] based on the optimized structure on the right of Figure S37 (higher-minimum structure), which has the dihedral angle of O(1)-Fe-O(2)-O(3) as 158º (See Figure S37 for atom labeling). But, in this study, we took a closer look at the rotation of $O_2CCF_3^-$ along the Fe-O(2) bond. We preformed a potential energy surface scan along a dihedral angle coordinate (dihedral angle O(1)-Fe-O(2)-O(3)) and found that two stationary points, which have dihedral angle τ [O(1)-Fe-O(2)-O(3)] = ± 47º (the structure on the left of Figure S38, lower-minimum structure), have same electronic energies that are ~ 1300 cm^{-1} lower than that of the higher-minimum structure (Figure S38). The comparison of geometric parameters of the first coordinate sphere of the iron center between these structures is shown in Table S16. We notice that the major differences are the Fe-O(2) bond length and the angles involving this bond. Despite of the large difference in electronic energies for the saddle-point and the minimum-point structures, the DFT calculated electronic properties are rather similar (See Table S17 and S18). Therefore, the DFT results of $[Fe^{IV}(O)(TPA)(O_2CCF_3)]^+$ published in [19] are still valid. Given the available experimental data and the accuracy of the current DFT calculations, one cannot determine which structure is more favorable. However, since the lower-minimum structure has much lower electronic energy, we presented DFT calculated parameters based on this structure in this study.

This journal is © The Royal Society of Chemistry 2012

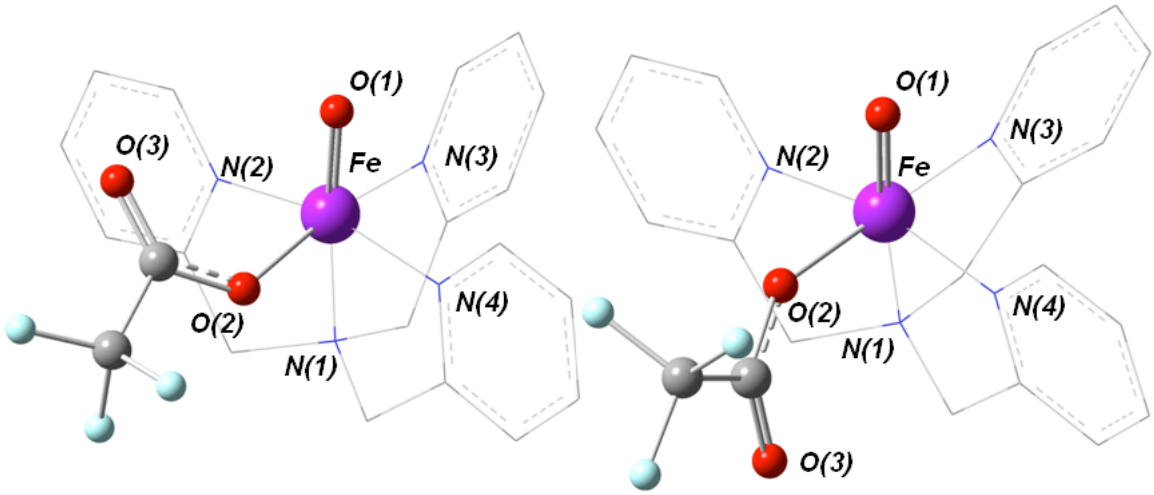

Figure S37. DFT optimized structures for $[Fe^{IV}(O)(TPA)(O_2CCF_3)]^+$ at the lower-minimum (left) and the higher minimum (right) of the potential energy surface (PES) shown in Figure S38. To highlight the structural differences, Fe^{IV}=oxo and the $O_2CCF_3^-$ units are represented by ball and stick model and the rest of the molecules are represented by wireframe model. Color code: Fe, magenta; C: grey; O, red; N, blue; F, light blue.

This journal is © The Royal Society of Chemistry 2012

Table S17. Selected Bond Lengths and Angles from DFT Optimized $[Fe^{IV}(O)(TPA)(O_2CCF_3)]^+$ in the Lower-Minimum Structure and the Higher-Minimum Structure Indicated in Figure S37. [a]

Selected bond lengths (Å) and angles (°)	**$[Fe^{IV}(O)(TPA)(O_2CCF_3)]^+$**	
	Saddle-Point	Minimum-Point
Fe-O(1)	1.64758	1.64590
Fe-O(2)	*1.95146*	*1.91684*
Fe-N(1)	2.12801	2.12625
Fe-N(2)	1.98460	1.97863
Fe-N(3)	1.99960	2.00110
Fe-N(4)	1.97704	1.98695
O(1)-Fe-N(1)	171.420	173.984
O(1)-Fe-N(2)	98.468	98.521
O(1)-Fe-N(3)	89.686	91.952
O(1)-Fe-N(4)	98.142	96.999
O(1)-Fe-O(2)	*91.610*	*99.991*
O(2)-Fe-N(1)	*96.882*	*85.826*
O(2)-Fe-N(2)	*85.609*	*89.481*
O(2)-Fe-N(3)	*178.694*	*168.015*
O(2)-Fe-N(4)	*90.499*	*85.891*
N(1)-Fe-N(2)	81.028	82.962
N(1)-Fe-N(3)	81.825	82.208
N(1)-Fe-N(4)	83.061	81.811
N(2)-Fe-N(3)	94.355	89.729
N(2)-Fe-N(4)	163.034	164.364
N(3)-Fe-N(4)	89.163	91.711

[a] Please refer to Figure S37 for the atom labeling; the Fe-O(2) bond length and the angles involving this bond are in italic.

This journal is © The Royal Society of Chemistry 2012

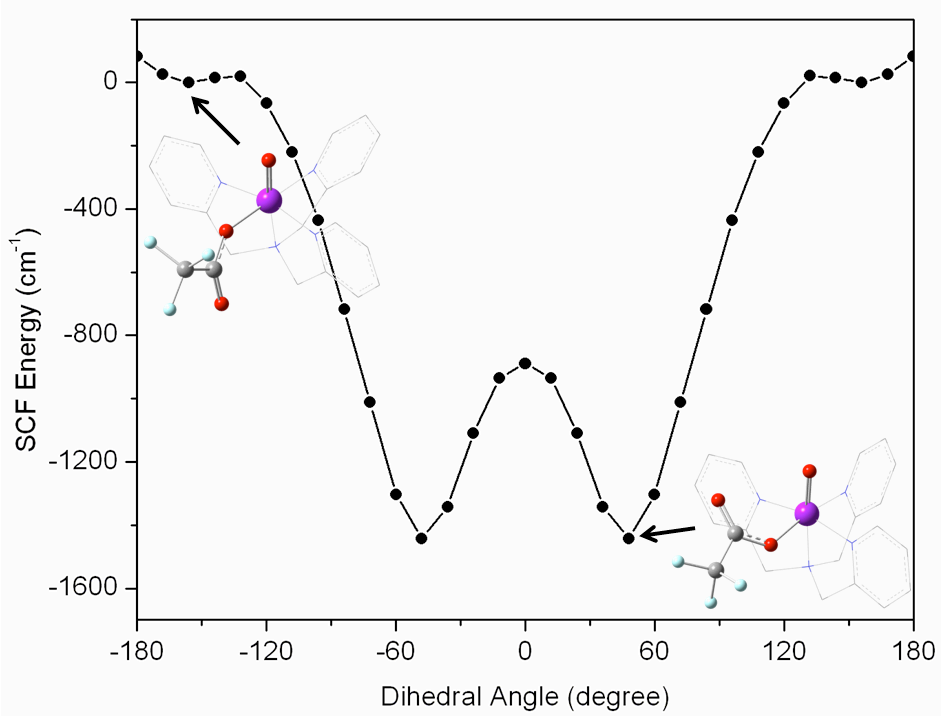

Figure S38. A section of the potential energy surface of $S = 1$ $[Fe^{IV}(O)(TPA)(O_2CCF_3)]^+$ with respect to the dihedral angle O(1)-Fe-O(2)-C(1) obtained by DFT calculations.

Table S18. DFT Calculated Properties of $[Fe^{IV}(O)(TPA)(O_2CCF_3)]^+$ Based on the Saddle-Point Structure and the Minimum-Point Structure.

	$[Fe^{IV}(O)(TPA)(O_2CCF_3)]^+$		
	Exp	Higher-Minimum	Lower-Minimum
δ (mm/s)	0.02	0.08	0.06
ΔE_Q (mm/s)	0.92	1.12	1.21
r(Fe-O(1)) (Å)	1.66	1.648	1.646
r(Fe-N) (Å)	1.98	2.023	2.023
r(Fe-O(2)) (Å)	1.98	1.951	1.917

This journal is © The Royal Society of Chemistry 2012

Table S19. Orbital Populations of d Orbitals and ΔE_Q Values of $[Fe^{IV}(O)(TPA)(O_2CCF_3)]^+$.

	orbital populations [a]						ΔE_Q		
	xy	xz	yz	x^2-y^2	z^2		est.[a]	DFT	exp
Higher-Minimum-Point	1.917	1.423	1.408	0.578	0.828		1.00	1.12	1.92
Lower-Minimum-Point	1.915	1.406	1.414	0.596	0.831		1.08	1.21	0.92

[a] Quadrupole splitting are estimated with the simple expression $\Delta E_Q(\text{est.}) = \Sigma_d\, P(d)V_{zz}(d)$, where $V_{zz}(d) = -4$ ($d=z^2$), 4 (x^2-y^2), 4 (xy), -2 (yz), -2 (xz) mm/s and P(d) is the population of orbital d.

This journal is © The Royal Society of Chemistry 2012

Table S20. Cartesian Coordinates of DFT Optimized Structure of Complex **5(b)** in the *S* =1 spin state.

Fe	-1.59279	-0.72882	-0.03844
N	0.200168	-0.08738	-0.97006
C	0.904257	-1.35131	-1.38584
H	1.679199	-1.59829	-0.66479
H	1.386176	-1.22264	-2.3522
C	-0.03853	-2.56911	-1.45798
O	0.375114	-3.59945	-2.01346
O	-1.20192	-2.42599	-0.84515
C	-0.20126	0.761079	-2.1416
H	0.415318	0.533542	-3.00898
H	-0.0571	1.815409	-1.90842
C	-1.68689	0.577947	-2.52356
O	-2.09161	1.098464	-3.57497
O	-2.42434	-0.08844	-1.6492
C	0.802514	0.675467	0.21555
C	0.83905	-0.35534	1.360566
C	1.838172	-0.51123	2.315955
H	2.723604	0.104512	2.292971
C	1.679015	-1.48803	3.306176
H	2.448274	-1.62867	4.052192
C	0.529596	-2.27812	3.321739
H	0.386674	-3.04109	4.071528
C	-0.4455	-2.07193	2.348082
H	-1.36797	-2.62724	2.292732
N	-0.28075	-1.12663	1.403095
C	-0.29887	1.682992	0.627866
C	-0.11713	3.00758	1.016641
H	0.865837	3.450308	1.036466
C	-1.2378	3.766776	1.373588
H	-1.11528	4.798602	1.670875
C	-2.5069	3.189427	1.338017
H	-3.38633	3.755958	1.603164
C	-2.63129	1.858768	0.945716
H	-3.56979	1.331061	0.890974
N	-1.5434	1.140465	0.607699
C	2.140103	1.395426	-0.06189
H	1.935044	2.21056	-0.76061
H	2.457276	1.877384	0.868708
C	3.323229	0.578912	-0.61506
H	3.094956	0.229232	-1.62325
H	3.502096	-0.31485	-0.01108

This journal is © The Royal Society of Chemistry 2012

C	4.615523	1.416833	-0.66302
H	4.432948	2.326874	-1.24453
H	4.871125	1.747406	0.350248
C	5.80102	0.652032	-1.26829
H	6.701378	1.268306	-1.2828
H	5.590361	0.347671	-2.2959
H	6.024969	-0.25069	-0.69483
O	-2.91831	-1.14434	0.847293

References:

1. M. Renz, C. Hemmert and B. Meunier, *Eur. J. Org. Chem.*, 1998, 1271-1273.
2. D. Macikenas, E. Skrzypczak-Jankun and J. D. Protasiewicz, *J. Am. Chem. Soc.*, 1999, **121**, 7164-7165.
3. W. L. F. Armarego and D. D. Perrin, *Purification of Laboratory Chemicals*, Butterworth-Heinemann, Oxford, 1997.
4. M. Lubben, A. Meetsma, E. C. Wilkinson, B. Feringa and L. Que, Jr., *Angew. Chem. Int. Ed. Engl.*, 1995, **34**, 1512-1514.
5. F. B. Abeles, P. W. Morgan and J. Mikal E. Saltveit, *Ethylene in Plant Biology*, Academic Press, San Diego, 1992.
6. Bruker Analytical X-ray Systems, Madison, WI, V5.054 edn., 2001.
7. R. Blessing, *Acta Cryst.* , 1995, **A51**, 33-38.
8. Bruker Analytical X-Ray Systems, Madison, WI, V6.45 edn., 2003.
9. Bruker Analytical X-Ray Systems, Madison, WI, V6.14 edn., 2000.
10. A. L. Spek, *PLATON. A multipurpose crystallographic tool*, Utrecht University, Utrecht, The Netherlands, 2002.
11. G. N. George and I. J. Pickering, Stanford Synchrotron Radiation Laboratory, Stanford Linear Accelerator Center, Stanford, California, 2000.
12. B. Ravel and M. Newville, *J. Synchrotron Radiation*, 2005, **12**, 537-541.
13. T.-C. Weng, G. S. Waldo and J. E. Penner-Hahn, *J. Synchrotron Radiation*, 2005, **12**, 506-510.
14. T. E. Westre, P. Kennepohl, J. G. DeWitt, B. Hedman, K. O. Hodgson and E. I. Solomon, *J. Am. Chem. Soc.*, 1997, **119**, 6297-6314.
15. J. J. Rehr, J. Mustre de Leon, S. I. Zabinsky and R. C. Albers, *J. Am. Chem. Soc.*, 1991, **113**, 5135-5140.
16. G. W. T. M. J. Frisch, H. B. Schlegel, G. E. Scuseria, M. A. Robb, J. R. Cheeseman, G. Scalmani, V. Barone, B. Mennucci, G. A. Petersson, H. Nakatsuji, M. Caricato, X. Li, H. P. Hratchian, A. F. Izmaylov, J. Bloino, G. Zheng, J. L. Sonnenberg, M. Hada, M. Ehara, K. Toyota, R. Fukuda, J. Hasegawa, M. Ishida, T. Nakajima, Y. Honda, O. Kitao, H. Nakai, T. Vreven, J. A. Montgomery, Jr., J. E. Peralta, F. Ogliaro, M. Bearpark, J. J. Heyd, E. Brothers, K. N. Kudin, V. N. Staroverov, R. Kobayashi, J. Normand, K. Raghavachari, A. Rendell, J. C. Burant, S. S. Iyengar, J. Tomasi, M. Cossi, N. Rega, J. M. Millam, M. Klene, J. E. Knox, J. B. Cross, V. Bakken, C. Adamo, J. Jaramillo, R. Gomperts, R. E. Stratmann, O. Yazyev, A. J. Austin, R. Cammi, C. Pomelli, J. W. Ochterski, R. L.

Electronic Supplementary Material (ESI) for Chemical Science
This journal is © The Royal Society of Chemistry 2012

Martin, K. Morokuma, V. G. Zakrzewski, G. A. Voth, P. Salvador, J. J. Dannenberg, S. Dapprich, A. D. Daniels, Ö. Farkas, J. B. Foresman, J. V. Ortiz, J. Cioslowski, and D. J. Fox Gaussian, Inc., Wallingford, CT, 2009.

17. E. J. Klinker, J. Kaizer, W. W. Brennessel, N. L. Woodrum, C. J. Cramer and L. Que, Jr., *Angew. Chem. Int. Ed.*, 2005, **44**, 3690-3694.
18. V. Vrajmasu, E. Münck and E. L. Bominaar, *Inorg. Chem.*, 2003, **42**, 5974-5988.
19. J.-U. Rohde, A. Stubna, E. L. Bominaar, E. Münck, W. Nam and L. Que, Jr., *Inorg. Chem.*, 2006, ***45***, 6435-6445.
20. J.-U. Rohde, S. Torelli, X. Shan, M. H. Lim, E. J. Klinker, J. Kaizer, K. Chen, W. Nam and L. Que, Jr., *J. Am. Chem. Soc.*, **2004**, ***126***, 16750-16761.
21. A. Chanda, X. Shan, M. Chakrabarti, W. C. Ellis, D. L. Popescu, F. Tiago de Oliveira, D. Wang, L. Que, T. J. Collins, E. Münck and E. L. Bominaar, *Inorg. Chem.*, 2008, **47**, 3669-3678.
22. F. Neese and E. I. Solomon, *Inorg. Chem.*, 1998, **37**, 6568-6582.